arTs Università degli Studi di Trieste
Archivio della ricerca – postprint

# Geochemistry and geochronology of dolerite dykes from the Daba and Dongbo peridotite massifs, SW Tibet: Insights into the style of mantle melting at the onset of Neo-Tethyan subduction

Chen Cheng [a], Hao Zheng [a,*], Argyrios Kapsiotis [a], Weiliang Liu [a], Davide Lenaz [b], Matteo Velicogna [b], Lifeng Zhong [a], Qiangtai Huang [a], Yajuan Yuan [a,*], Bin Xia [a]

[a] Key Laboratory of Offshore Oil Exploration and Development of Guangdong Higher Education Institutes, Guangdong Provincial Key Laboratory of Marine Resources and Coastal Engineering, School of Marine Science,Sun Yat-sen University, Guangzhou 510275, China
[b] Department of Mathematics and Geosciences, University of Trieste, Via Weiss 8, Trieste 34128, Italy

ARTICLE INFO

Accepted 21 October 2018

*Keywords:*
Dolerite dykes
Ophiolites
Daba
Dongbo
Tibet
Neo-Tethys

ABSTRACT

This study reports on compositional, whole-rock Sr—Nd isotopic, and zircon U—Pb geochronological data for dolerite dykes in the Daba and Dongbo ultramafic massifs of the southwest Yarlung–Zangbo Suture Zone (YZSZ), SW Tibet. The 121 ± 2 Ma dolerite dykes from the Daba peridotite exhibit primitive mantle (PM)-normalised multi-element patterns with $(La/Yb)_N = 0.43–0.72$ and negative Nb anomalies. They have high initial $^{87}Sr/^{86}Sr$ ratios ($^{87}Sr/^{86}Sr_{(i)} = 0.707197$ to 0.707879) and high $\varepsilon_{Nd}(t)$ values (+7.4 to +7.9). The 125 ± 2 Ma dolerite intrusions within the Dongbo peridotite show PM-normalised trace element profiles [$(La/Yb)_N = 0.65–0.84$] that are characterised by apparent negative Nb anomalies and moderate negative Ti (±Y) anomalies. They also have high $^{87}Sr/^{86}Sr_{(i)}$ ratios (0.706108–0.706793) and high $\varepsilon_{Nd}(t)$ values (+7.8 to +8.2). Semi-quantitative Sm/Yb vs. La/Sm modelling demonstrates that the parental magmas of the investigated dykes were derived from 10%–20% (cumulative) melting of a (broad) mantle source region that had a spinel-bearing normal mid-ocean ridge basalt (N-MORB)-like lherzolitic composition. The geochemical and isotopic data indicate that the composition of the inferred mantle source was influenced by minor inputs of subducted crustal material. The petrogenesis of the Daba and Dongbo massifs can be linked to the upwelling of an asthenospheric source that caused continental rifting and subsequent seafloor spreading that was followed by the subduction initiation adjacent to a passive margin during the Early Cretaceous (~130–120 Ma). The results provide a more detailed and perhaps more elegant hypothesis for the tectonomagmatic evolution of the southwestern YZSZ "ophiolitic" peridotites after their accretion beneath a Neo-Tethyan marginal basin.

## 1. Introduction and rationale

The interpretation of on-land ophiolite suites of rocks as the petrological analogues of the present-day oceanic lithosphere has ignited interest in the investigation of ophiolites during recent decades (Bédard et al., 2009; Dilek and Furnes, 2014; Stern and Bloomer, 1992). With the advent of plate tectonics theory, ophiolites have been interpreted as slices of fossil oceanic lithosphere trapped along consuming plate margins during continental collision and the subsequent building of large orogenic systems (Coleman, 1977; Gass et al., 1990). Consequently, ophiolites can help us understand complicated petrological processes within modern oceanic basins, and they play a significant role in the decoding of geodynamic mechanisms that control the assembly of large landmasses (e.g., Dilek and Furnes, 2011).

In most orogenic belts, ophiolite assemblages occur as allochthonous sequences that were emplaced tectonically onto the continental margin (e.g., Moghadam and Stern, 2011), and some typical examples of imbricated ophiolites are those that crop out along the (Indus) Yarlung Zhangbo Suture Zone [(I)YZSZ] in the Himalayas. This immense suture zone marks the collision between the northwards-drifting Indian Plate and the Eurasian Plate during the Mesozoic–Cenozoic closure of the Neo-Tethys (Aitchison et al., 2000). During the last four decades, a great amount of knowledge on the origin of Neo-Tethyan ophiolites has been accumulated by detailed investigations on the petrogenesis of

* Corresponding authors.
*E-mail addresses:* zhengh66@mail.sysu.edu.cn (H. Zheng), yuanyaj3@mail.sysu.edu.cn (Y. Yuan).

the YZSZ oceanic massifs (e.g., Bédard et al., 2009; Dupuis et al., 2005; Girardeau et al., 1985; Hébert et al., 2012; McGowan et al., 2015; Nicolas et al., 1981; Pearce and Deng, 1988; Wu et al., 2014; Zhou et al., 1996, 2005).

Various tectonomagmatic scenarios has been invoked to explain the petrological evolution of the YZSZ ophiolites within the eastern realm of the Neo-Tethyan Ocean (Hébert et al., 2012). The early models involved the formation of the YZSZ ophiolites at a slow-spreading mid-ocean ridge (MOR) similar to that in the southwestern part of the present-day Indian Ocean (e.g., Girardeau and Mercier, 1988; Nicolas et al., 1981).The more recent models have ascribed the petrogenesis of the YZSZ ophiolites to igneous accretion that took place in a wedge above an intra-oceanic subduction zone setting similar to that beneath the Izu–Bonin–Mariana arc system of the West Pacific Ocean (Aitchison et al., 2000; Bédard et al., 2009; Dupuis et al., 2005; Hébert et al., 2012; Wang et al., 2000; Zheng et al., 2017; Zhou et al., 2005).

Despite significant progress in understanding the origin of the YZSZ ophiolites, several aspects of their petrogenesis remain puzzling: i) there is a remarkable paucity of pillow lavas and sheeted dykes in the YZSZ ophiolites (Griffin et al., 2016), ii) there is a geochemical and isotopic decoupling of the YZSZ peridotite massifs from their immediate crustal lithologies (Liu et al., 2012; Wu et al., 2014), iii) mafic rocks with ocean island basalt (OIB)-type geochemical affinities are found in some of these ophiolites (e.g., Bézard et al., 2011; He et al., 2016; Xia et al., 2008), and iv) there is an extensive assortment of unusual trace minerals [i.e., super-reducing–ultra-high pressure (SuR–UHP) minerals] in some of the Tibetan chromitites (McGowan et al., 2015) and peridotites (Yang et al., 2011). These findings are difficult to reconcile with previous models of the geological history of the YZSZ ophiolites, and it is therefore necessary to undertake a more detailed examination of the geodynamic processes that contributed to the opening and destruction of the Neo-Tethyan seaway in the broader Tibetan region.

Herein, a detailed report is provided on the geological, petrographic, geochemical and Sr—Nd isotopic data for the mafic dyke intrusions in the Daba and Dongbo peridotite massifs (SW Tibet). New U—Pb geochronological data are presented for magmatic zircons separated from these mafic intrusions, thus providing a critical temporal link between the igneous accretion of these peridotite massifs and the tectonics of the Eurasian active margin during the Early Cretaceous. The data reveal important petrogenetic links between the extension of the lithospheric mantle and the intrusion of the mafic dykes. These data, integrated with the results of recent studies, provide insights into the enigmatic petrotectonic evolution of the southwestern segment of the YZSZ.

## 2. Geological setting

The Tibetan Plateau, often called the “roof of the world”, is a collage of continental terranes that were added successively to the southern margin of the Eurasian Plate during the Paleozoic and Mesozoic (Aitchison et al., 2000). These exotic continental fragments are separated by a series of well-defined E–W trending suture zones marked by scattered occurrences of ophiolitic material that was caught up between the continental blocks during collision (Yin and Harrison, 2000; Fig. 1a). From north to south, these are the Kunlun Suture Zone (KSZ), the Garzê–Litang Suture Zone (GLS), the Jinsha Suture Zone (JSSZ), the Longmu Tso–Shuanghu Suture Zone (LSSZ), the Bangong–Nujiang Suture Zone (BNSZ), and the Yarlung Zangbo Suture Zone (YZSZ). These zones represent the remnants of the Tethyan Ocean (for a review, see Zhang et al., 2004). The ~2000 km-long YZSZ is the southernmost of the suture zones in Tibet, representing the line of collision between the Indian Plate to the south and the Lhasa–Karakoram Block to the north (e.g., Ji et al., 2009). This gigantic tectonic boundary is marked by a series of discontinuous outcrops of ophiolite and associated mélanges that are interpreted to be the remnants of the Neo-Tethyan Ocean (Hu et al., 2016; Fig. 1a).

The YZSZ is divided structurally into three segments: i) the eastern segment, which extends from the eastern Himalaya syntaxis to Xigaze and which was strongly affected by N—S compression during and after the collision between India and Asia (Xu et al., 2015); ii) the central segment, which extends from Xigaze to Saga in the west and which was juxtaposed against a Cretaceous–Eocene forearc basin sequence to the north that does not exist in the other two segments (e.g., Liu et al., 2018a);and iii) the western segment, which begins at Saga in the east and ends in the Ladakh Batholith (Fig. 1b).The western segment of the YZSZ is further divided by the ~900 km-long and ~100 km-wide continental Zhongba–Zhada Terrane into two subparallel ophiolite belts: i) a northwestern ophiolite belt that is tectonically juxtaposed against an accretionary prism complex and the Eurasian Gangdese arc (>150 to 35 Ma; Harrison et al., 2000) along dextral oblique-slip faults, with the ophiolites cropping out as discontinuous lensoidal bodies within a block-in-matrix mélange with a serpentine-rich groundmass (e.g., Liu et al., 2018a); and ii) a southwestern ophiolite belt in southwestern Tibet that tectonically overlies the Tethyan Himalaya sequence in the south (Pan et al., 2004; Fig. 1b) and forms a ~300 km-long discontinuous belt that is dominated by a series of large peridotite massifs; from east to west, the Zhongba, Dangqiong, Xiugugabu, Zhaga, Purang (Yungbwa), Dongbo (Kiogar) and Daba massifs. These massifs crop out to the south of the YZSZ and are locally thrust northwards onto the Zhongba–Zhada Terrane (e.g., Liu et al., 2018a and references therein; Fig. 1b).

### 2.1. Daba and Dongbo ophiolites

The Daba ophiolite is a ~1 km wide and ~8 km long ultramafic massif, consisting mainly of fault-bounded peridotite slivers (Fig. 1c) intruded by mafic dyke swarms (Fig. 2a). Unlike the ideal Penrose-type ophiolite, a cumulate sequence and a sheeted dyke complex are missing in Daba, and this is a common feature of the ophiolitic massifs in the southwestern part of the YZSZ. Underneath the peridotites is a thin Jurassic–Cretaceous mélange (Yang et al., 2011; Fig. 1c) that consists of dismembered peridotite and slices of volcanic rock and shallow to bathypelagic limestone within a serpentine-rich matrix. Locally, radiolarian cherts rest nonconformably on the mantle peridotites (Fig. 2a–c). The exact age of the massif remains unknown since paleontological and geochronological data have yet to be reported from Daba.

The Dongbo ophiolite, in the Ali area, is one of the largest oceanic massifs cropping out in the southwestern segment of the YZSZ (Fig. 1c). Aeromagnetic data show that the Dongbo massif covers an area of >400 $km^2$, though almost one-third of the massif is covered by Neogene to Quaternary sedimentary deposits (Niu et al., 2015). The massif consists generally of a large peridotite body associated with minor crustal lithologies overlying a Cretaceous tectonic mélange (Yang et al., 2011; Fig. 1c). More specifically, the Dongbo mantle sequence is composed of variably depleted harzburgites (Fig. 2d), and it locally hosts small and irregularly shaped bodies of lherzolite and dunite (Xiong et al., 2017). The dunite commonly hosts imbricated pods and lenses of (metallurgical and refractory) chromitite (Xiong et al., 2017). The peridotites are locally intruded by mafic dyke swarms (pyroxenite, gabbronorite and dolerite; Xiong et al., 2011; Fig. 2d, e). A volcano–sedimentary sequence (200–500 m thick) of basaltic lava flows and pyroclastic (silicic tuffaceous) lithologies rests locally on the mantle peridotites (Liu et al., 2015a). In the absence of extrusive lithologies, the (eroded) mantle sequence is unconformably overlain by radiolarites (Niu et al., 2015; Fig. 2d–f). A Cretaceous tectonic mélange that contains exotic blocks of serpentinised peridotite, extrusive rocks, Triassic carbonates, and clastic lithologies occurs at the base of the massif (Xiong et al., 2011; Yang et al., 2011; Fig. 1c).

The absence of a sub-ophiolitic metamorphic sole indicates that the Dongbo ophiolite is a coherent massif without significant evidence of internal dismemberment during its original displacement and

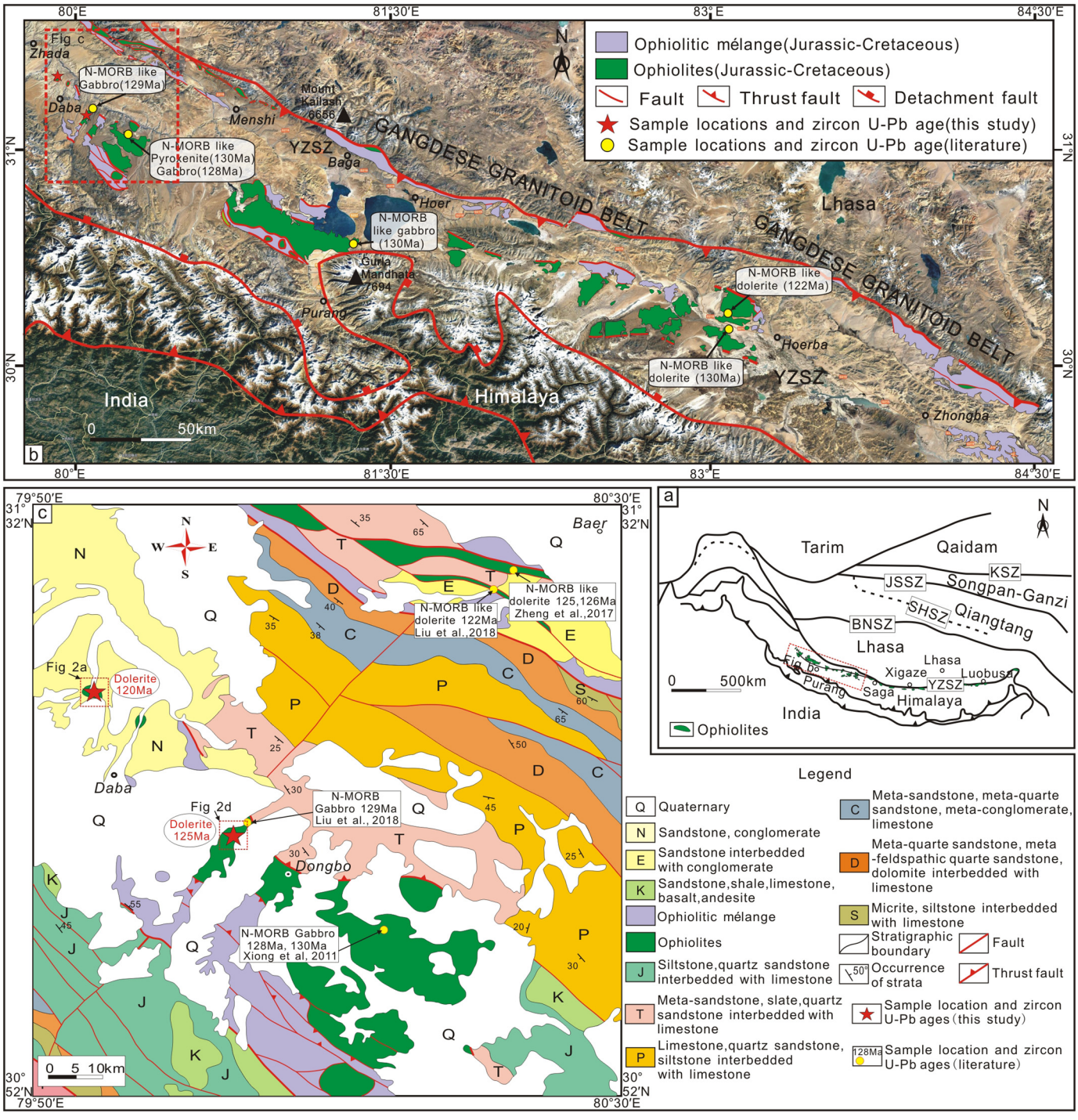


**Fig. 1.** a) Schematic tectonic framework of the Tibetan Plateau (after Zhang et al., 2004) showing major tectonic subdivisions; b) Geographic-geological map showing the ophiolite outcrops along the western segment of the YZSZ (modified from Satellite image). c) Geological sketch map of the Daba and Dongbo ultramafic massifs (modified after Yang et al., 2011).Abbreviations: YZSZ = Yarlung Zangbo Suture Zone; BNSZ = Bangong–Nujiang Suture Zone; SHSZ = Shuanghu Suture Zone; JSSZ = Jinshajiang Suture Zone; KSZ = Kunlun Suture Zone (a). Yellow circles are sample locations reported from Bao et al. (2015), Liu et al. (2011), Liu et al. (2018a,2018b), Wei et al. (2006), Xiong et al. (2011) and Zheng et al. (2017). The locations of the investigated samples are also marked as red asterisks (c). (For interpretation of the references to colour in this figure legend, the reader is referred to the web version of this article.)

subsequent tectonic incorporation into the northern continental margin of India.

U—Pb isotope dilutionthermal ionisation mass spectrometry (ID–TIMS) dating of a single zircon crystal recovered from a gabbronorite dyke at Dongbo yielded an age of 159.7 ± 0.5 Ma (Chan et al., 2015). However, U—Pb multicollector–laser ablation–inductively coupled plasma–mass spectrometry (MC–LA–ICP–MS) dating of zircons separated from pyroxenite and gabbro intrusions within the Dongbo peridotites yielded crystallisation ages of 130.4 ± 0.5 and 128.5 ± 1.1 Ma, respectively (Xiong et al., 2011).

## 3. Sampling and field observations

During regional-scale field work, four samples of mafic dykes were collected from a peridotite suite to the north of Daba village (31°19′N, 79°54′E) and six samples of mafic intrusions from a

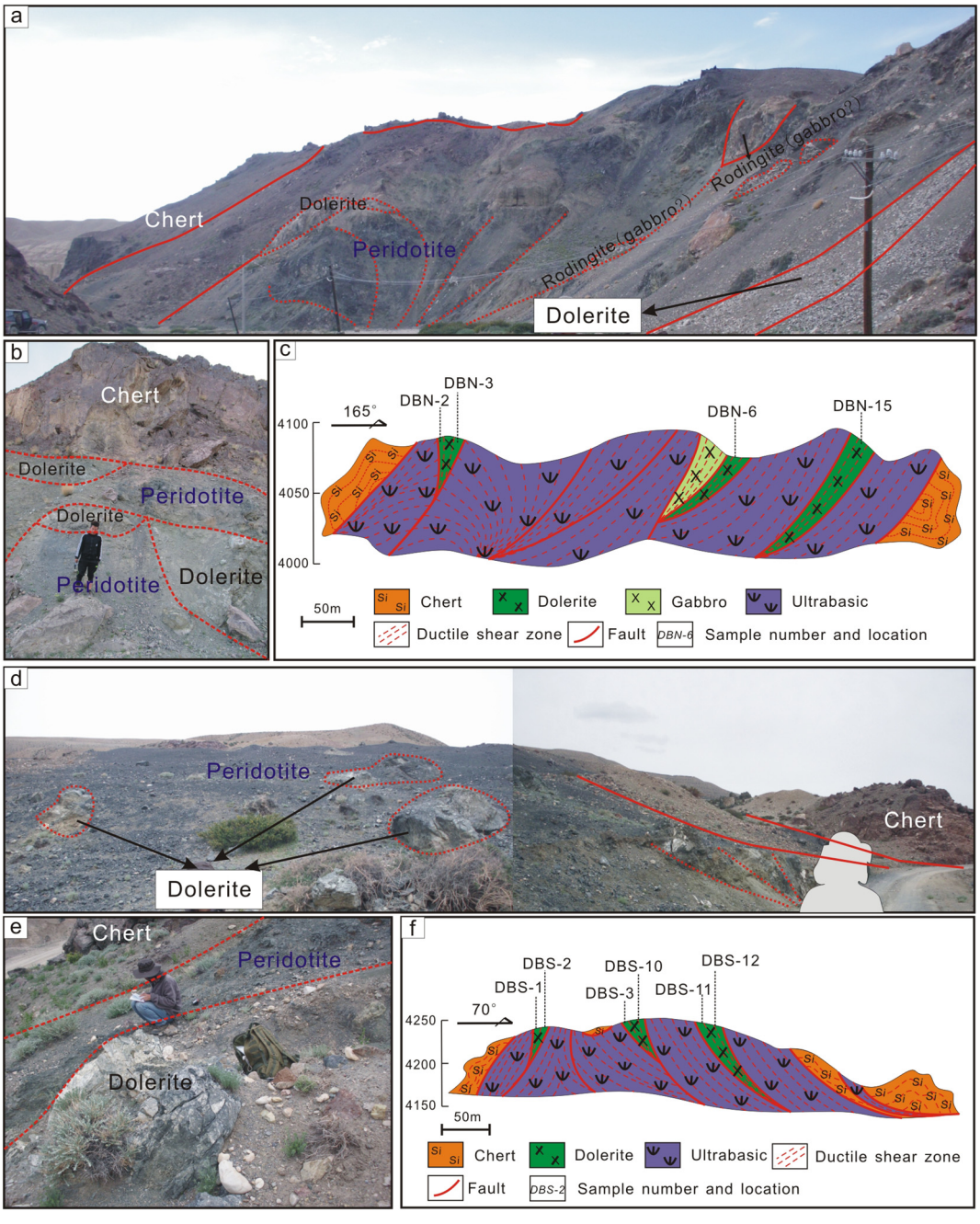


**Fig. 2.** Field photos and cross sections showing the geological relationship between mafic dykes/intrusive bodies, peridotites and radiolarites in the Daba (a-c) and Dongbo (d-f) ultramafic massifs.

well-exposed ultramafic suite to the northwest of Dongbo hamlet (31°10′N, 80°04′E; Fig. 1c). Samples were taken from the least-altered mafic dykes. Mafic dykes from both study areas are similar; consequently, their macroscopic features are described as if they form a single group of rocks, but at the same time their differences are highlighted.

The Daba and Dongbo regions are extremely mountainous, lying at altitudes higher than 4100 and 4200 m, respectively. Mafic dykes are common within the Daba and Dongbo peridotites, occurring mainly in amphitheatre-like valleys, emplaced along major fractures with moderate dips. They lack distinct mineralogical or textural layering and do not bifurcate, indicating they are independent of each other.Furthermore, no dyke was observed to cut any other dyke.

The maximum distance over which an individual dyke is traceable ranges from several tens of metres to a few hundreds of metres (Fig. 2). Mafic dykes at Daba are generally thicker than those at Dongbo (~5–25 and ~1–5 m, respectively). Most of the mafic dykes are tabular and they have smooth planar contacts with the host peridotite. The peridotites in both massifs show a blackened zone that is rich in serpentine (±chlorite) along the contacts with dykes, thus enveloping the intrusions. At Dongbo, the mafic dykes show chilled margins against their host rocks, and relatively coarse-grained centres. Large (≤0.7 mm) euhedral crystals are commonly observed in the interior of those dykes, indicating that the crystallisation was initiated after the emplacement of the dyke material at the currently exposed erosion level.

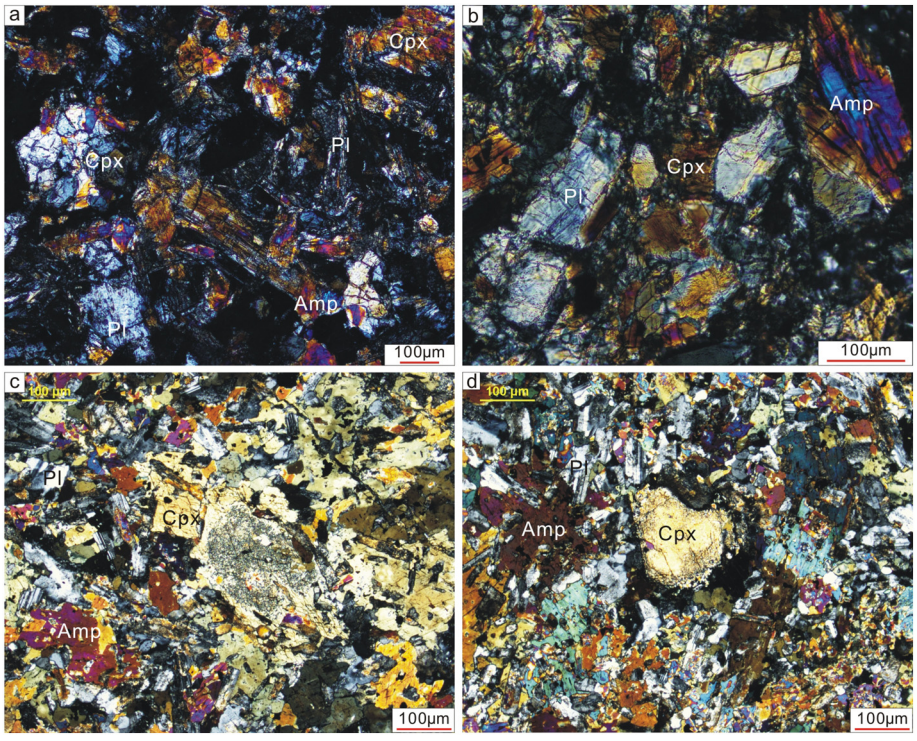


**Fig. 3.** a-b) Photomicrographs of dolerite dykes from the Daba ultramafic massif. Note the replacement of clinopyroxene by tremolite (a-b). Also note that plagioclase and clinopyroxene show minor undulose extinction and are often cross cut by a network of intragranular brittle micro-fractures (b). Yellow interference colors of plagioclase crystals generally imply a thick section (b). c-d) Photomicrographs of dolerite dykes from the Dongbo ultramafic massif, showing ophitic (c) to intergranular texture (d). All photos were taken under crossed polarized transmitted light. Abbreviations (in alphabetical order): Amp – amphibole; Cpx – clinopyroxene; Pl – plagioclase. (For interpretation of the references to colour in this figure legend, the reader is referred to the web version of this article.)

The investigated mafic dykes crosscut superficially weathered harzburgites (Fig. 2a, b, d, e) that locally retain fossil WNW–ESE-oriented $S_0$ asthenospheric/diapiric fabrics (Nicolas et al., 1981) and NE–SW-trending stretching lineations (defined by elongate grains of pyroxene and spinel). The areas of harzburgite that preserve the high-*T* mantle fabrics have been passively translated by NW–SE-striking low-*T* ductile shearing along planar zones of mylonite. These structural relationships indicate that the shear zones in both study areas reflect the SW-directed displacement of an oceanic lithospheric slab, rather than the original asthenospheric deformation, and that the mafic dykes formed within fractures that opened during inhomogeneous brittle to semi-brittle shearing in an intraoceanic setting. The investigated mafic intrusions also show evidence of low-*T* deformation in the form of late brittle structures such as minor neotectonic strike-slip faults.

Peridotites from both studied massifs host small (a few metres in size) and locally rodingitised gabbroic bodies, and the peridotites are locally overlain unconformably by radiolarites (Fig. 2a, d). This observation supports the idea that the Daba and Dongbo massifs have a cogenetic relationship. Consequently, an analysis of these massifs is expected to provide valuable temporal and compositional constraints on the life-cycle of the Neo-Tethyan seaway to the northwest of the passive margin of India during the Late Jurassic–Early Cretaceous.

## 4. Analytical methods

Two polished thin sections were cut from each of the 10 mafic dyke samples collected for this study. All the rock sections were examined under transmitted and reflected light, using an OLYMPUS BX51 conventional microscope at the School of Marine Science, Sun Yat-sen University (SYSU), Guangzhou (China).

All the mafic dyke specimens were analysed for their bulk-rock major-element oxide and trace element contents. Any visible altered and/or weathered rims were first sawn from the samples, and the fresh material was then crushed into smaller blocks and ultrasonically cleaned in distilled water with 3% $HNO_3$. Subsequently, the blocks were washed with purified water alone, and then dehydrated and handpicked to eliminate anthropogenic contamination. The blocks were then crushed and ground to <200 mesh in an agate ring mill, and the resultant powders were used for geochemical analysis. Major-element oxides were determined by X-ray fluorescence (XRF) using a Rigaku 100e spectrometer at the Guangzhou Institute of Geochemistry of the Chinese Academy of Sciences (GIGCAS), Guangzhou, China. Analyses of the United States Geological Survey (USGS) rock standard BHVO-2, AGV-2 and W-2a indicate precisions better than 2% for $SiO_2$, $TiO_2$, $Al_2O_3$, $Fe_2O_3$t and CaO, and better than 4% for the other major-element oxides. Loss on ignition (LOI) was measured by gravimetric techniques with a detection limit of 0.01 wt%. Trace element contents were also measured at the GIGCAS using a PE Elan 6000 inductively coupled plasma–mass spectrometer (ICP–MS). The USGS reference material AGV-2 and AMH-1 were employed to monitor the accuracy of the analyses. Analytical uncertainties were ± 5%–10% for trace elements and ± 5% for the lanthanide series of elements. The bulk-rock concentrations of major-element oxides, trace elements and lanthanides are given in Supplementary Table A1–1and A1–2.

The bulk-rock Sr—Nd isotopic compositions of the investigated mafic dykes were determined using a Neptune Plus (Thermo Fisher Scientific, MA, USA) MC–ICP–MS with nine Faraday cup collectors and eight ion counters at the GIGCAS. A thorough description of the analytical method is provided by Yang et al. (2006). $^{87}Sr/^{86}Sr$ and $^{143}Nd/^{144}Nd$ ratios were corrected for mass fractionation to $^{86}Sr/^{88}Sr = 0.1194$ and $^{146}Nd/^{144}Nd = 0.7219$, respectively. The exponential decay constants ($\lambda$) used were $1.42 \times 10^{-11}$ $a^{-1}$ for $^{87}Rb$ and $6.54 \times 10^{-12}$ $a^{-1}$ for $^{147}Sm$. The values of $\varepsilon_{Nd}(t)$ were calculated on the basis of the following present-day reference values for the chondritic uniform reservoir

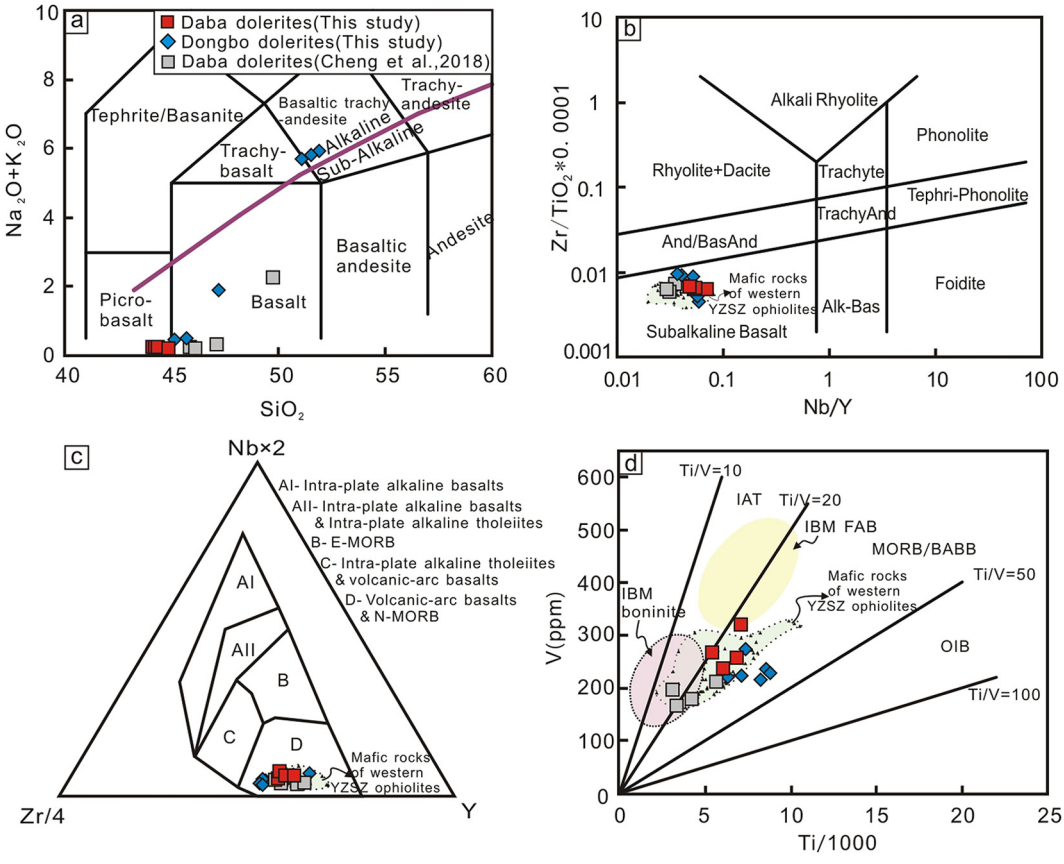


**Fig. 4.** a) $Na_2O + K_2O$ (wt%) vs. $SiO_2$ (wt%) (after LeBas et al., 1986), b) $Zr/TiO_2*10^{-4}$ vs. Nb/Y (after Winchester and Floyd, 1977), c)Nb*2-Zr/4-Y (after Meschede, 1986), d) V (ppm) vs. Ti/$10^3$ (after Shervais, 1982)for the Daba and Dongbo dolerite dykes. In (a) the alkaline-tholeiitic (/sub-alkaline) line is from Macdonald and Katsura (1964). In (d) data for Izu-Bonin-Mariana (IBM) boninites and fore-arc basalts (FAB) are from Reagan et al. (2010).Abbreviations (in alphabetical order):BABB = back-arc basin basalt; *E*-MORB = enriched mid-ocean ridge basalt; IAT = island arc tholeiite; IBM = Izu-Bonin-Mariana; OIB = ocean island basalt; MORB = mid-ocean ridge basalt. Literature data of mafic rocks from the western YZSZ ophiolites are also shown for comparison(Bao et al., 2015; Cheng et al., 2018; Guilmette et al., 2012; Liu et al., 2015a,b,2018a, b; Wei et al., 2006; Xiong et al., 2011; Zheng et al., 2017;).

(CHUR): $(^{143}Nd/^{144}Nd)_{CHUR} = 0.512638$ and $(^{147}Sm/^{144}Nd)_{CHUR} = 0.1967$. Bulk-rock Sr—Nd isotopic data are given in Supplementary Table A2.

Zircons were separated by conventional heavy-liquid and isodynamic magnetic methods at the GIGCAS. After separation, the zircons were handpicked under a binocular microscope, mounted in epoxy resin disks and polished until the grain centres were exposed. Zircons were imaged under reflected and transmitted light using an OLYMPUS BX51 optical microscope at the School of Marine Science, SYSU. Prior to undertaking the compositional analyses and geochronological dating, the microtextural characteristics of the zircons were studied in back-scattered electron (BSE) and cathodoluminescence (CL) images obtained with a CARL ZEISS SIGMA scanning electron microscope (SEM) at the School of Marine Science, SYSU. To avoid any effects of varying experimental conditions, each zircon was scanned for the same duration, and BSE and CL images were taken with constant signal amplification.

The lanthanide contents of zircons were determined by LA–ICP–MS using an Agilent 7500a ICP–MS coupled with a Resonetics RESOlution M-50 ArF Excimer laser source (wavelength/ë = 193 nm) at the State Key Laboratory of Isotope Geochemistry, GIGCAS. Analyses were carried out with a beam diameter of 33 ìm, a laser energy of 80 mJ, a frequency of 10 Hz and an ablation time of 40 s. External calibration was performed using a TEMORA zircon ($^{206}Pb/^{238}U$ age = 416.8 ± 1.3 Ma; Black et al., 2004) and a QINGHU zircon standard ($^{206}Pb/^{238}U$ age = 159.5 ± 0.2 Ma; Li et al., 2009). Quantitative analyses for several trace elements were performed through calibration of relative element sensitivities using the NIST-610 standard glass, and through the normalisation of each analysis to $^{29}Si$ that was used as the internal standard. Analytical uncertainties for most elements were <10%. Off-line raw data selection and the integration of background and peak signals, as well as time-drift correction and quantitative calibration for U—Pb dating, were performed using ICPMSDataCal (Liu et al., 2010b). The age calculations and concordia diagrams were made using Isoplot/Ex ver. 3.0 (Ludwig, 2003). All ages were calculated with 2ó errors. The concentrations of lanthanides and the U—Pb isotopic data for the zircons are presented in Supplementary Table A3, Table A4–1 and Table A4–2, respectively.

## 5. Result

### 5.1. Petrography

In hand-specimens, the mafic dykes from both study areas show a light to dim green colour and a pervasive isotropic, medium to coarse granular igneous fabric. However, under the microscope, the specimens from the two study areas display quite different mineralogical and microtextural characteristics. Consequently, their petrographic features are described separately in the following account.

Modal analyses of the Daba mafic intrusions gave averages of 45%–50% plagioclase (anorthite), 50%–55% clinopyroxene (augite) and accessory amounts of metallic minerals, leading to their classification as dolerites (Fig. 3a, b). These dolerites contain anhedral to subhedral crystals of plagioclase (≤0.5 mm) and clinopyroxene (≤0.7 mm) in a glassy to cryptocrystalline groundmass. The microstructural relationship between the phenocrysts and the glassy matrix gives rise to an intersertal

texture. Locally, very fine (≤60 μm) anhedral to subhedral crystals of opaque minerals (mainly Fe-rich oxides) are dispersed between the plagioclase and clinopyroxene laths. Plagioclase and clinopyroxene show weak undulose extinction and are often cut (and offset) by a network of randomly oriented intragranular micro-cracks (Fig. 3b). Although plagioclase is practically unaffected by post-magmatic alteration, the clinopyroxene is locally pseudomorphed by tremolitic amphibole (Fig. 3a, b).

Modal analyses of the Dongbo mafic dykes gave averages of 35%–45% plagioclase (anorthite), 35%–40% clinopyroxene (augite to titanaugite), 20%–25% amphibole (hornblende), and trace amounts of Fe—Ti oxides, resulting in their classification as dolerites (Fig. 3c, d). These dolerites commonly show ophitic (Fig. 3c) to medium-grained intergranular textures (Fig. 3d). Ophitic texture is the dominant type of microstructure in the centres of the Dongbo dolerite dykes, whereas intergranular texture is typical of their chilled margins. The inner parts of these dykes are occupied by large (≤0.7 mm) clinopyroxene and amphibole oikocrysts that poikilitically enclose randomly oriented plagioclase and oxide mineral chadacrysts (≤0.1 and ≤ 30 μm, respectively; Fig. 3c). In the chilled margins, the clinopyroxenes and amphiboles form anhedral phenocrysts (≤0.3 mm) that are surrounded by much smaller (≤70 μm) subhedral grains of plagioclase (Fig. 3d). This transition from intergranular to ophitic texture indicates lower rates of cooling and slower rates of nucleation from the chilled surfaces to the warmer interiors of the dykes. This is consistent with the observation that the clinopyroxene close to the contacts of dykes with the country rock is pleochroic to some extent, implying a significant Ti-content (titanaugite), and therefore conditionsof rapid cooling. Augite phenocrysts in the chilled margins occasionally show corona textures, and less often concentric zoning. The Dongbo dolerite dykes were weakly affected by hydrothermal alteration, as a result of which the plagioclase was converted to fine-grained sericite, some clinopyroxene was partially replaced by actinolite and chlorite, and rarely, the amphibole was replaced by a fine-grained mixture of platy chlorite, quartz, Fe-oxides and calcite. The chloritisation generally increases near the boundaries of the investigated dolerite dykes.

Serpentinisation and rodingitisation are widespread in the Daba and Dongbo areas, but not pervasive, and these processes significantly affected the mineralogy of the gabbroic intrusive bodies within the peridotites of both study areas (Fig. 2a). The adjacent dolerite dykes were practically unaffected, as confirmed by field and petrographic observations. This implies that the emplacement of the dolerite dykes postdated the low-*T* alteration of the gabbros and their host harzburgites.

### 5.2. Geochemistry

Our petrographic observations show that the Daba and Dongbo dolerite dykes were affected to some extent by hydrothermal alteration and low-*T* metamorphism. This observation is consistent with their low to moderate loss on ignition (LOI) values (2.83–4.81 and 2.31–3.58 wt%, respectively). Therefore, only those elements that were not significantly affected by post-magmatic processes were used in the geochemical analysis. These include the incompatible trace elements Ti, Zr, Nb, Ta, Hf, Th, Y and V, as well as the lanthanides. The absence of a clear correlation between these elements and LOI values implies that their concentrations were not disturbed by post-magmatic processes.

The compositions of the dolerite dykes from the Daba massif vary in MgO (5.75–9.94 wt%) and $Al_2O_3$ (13.04–15.68 wt%; Table A1–1 in the supplementary file), and these variations are similar to those in the dolerite intrusions of the Dongbo massif (MgO = 5.00–9.31 wt%, $Al_2O_3$ = 13.22–16.33 wt%; Table A1–1 in the supplementary file). Despite their compositional similarities, the investigated dolerite dykes collectively do not comprise a geochemically homogeneous group of mafic intrusions. In fact, the dolerite intrusions from Daba are somewhat richer in CaO (15.35–20.10 wt%) and poorer in $TiO_2$ (0.53–1.20 wt%), $K_2O$ (0.02–0.03 wt%) and $P_2O_5$ (0.04–0.09 wt%) than those from Dongbo (CaO = 5.38–17.55 wt%, $TiO_2$ = 1.06–1.47 wt%, $K_2O$ = 0.07–0.26 wt%, $P_2O_5$ = 0.09–0.15 wt%; Table A1–1 in the supplementary file). Furthermore, the values of the magnesium number [$Mg^{\#} = 100 \times Mg/(Mg + Fe^{t})$] for the dolerite dykes from Daba range from 63 to 76, whereas those for the dolerite dykes from Dongbo vary from 51 to 70.

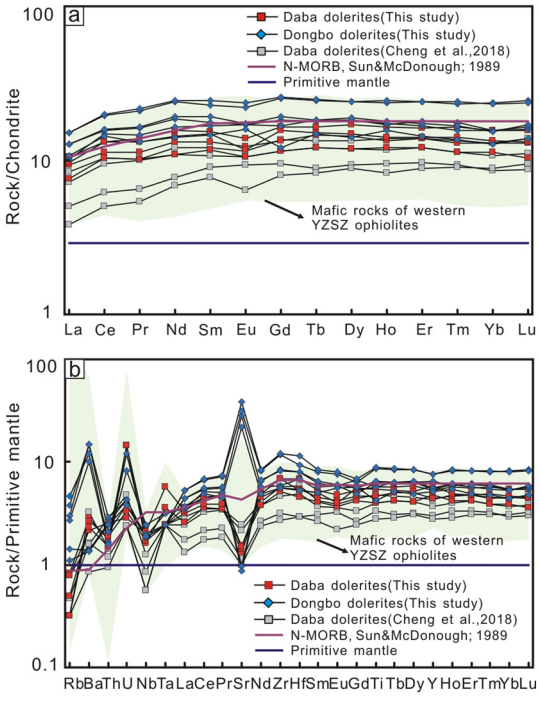


**Fig. 5.** a) Chondrite-normalised lanthanide profiles and b) primitive mantle (PM)-normalised multi-element profiles for the Daba and Dongbo dolerite dykes. The chondrite and primitive mantle (PM)-normalizing data are from Sun and McDonough (1989). Data of mafic rocks from the western YZSZ ophiolites are from the same sources as in Fig. 4.

On the $Na_2O + K_2O$ vs. $SiO_2$ diagram (Lebas et al., 1986), the mafic dykes are mostly sub-alkaline in composition, except for a group of dolerite intrusions from the Dongbo massif with a slight alkaline geochemical signature (Fig. 4a). However, on the logarithmic $Zr/TiO_2{*}10^{-4}$ vs. Nd/Y diagram (Winchester and Floyd, 1977) the dolerite dykes have an apparent sub-alkaline basalt composition (Fig. 4b).Furthermore, on the Nb*2–Zr/4–Y diagram (Meschede, 1986) the dolerite dykes plot in

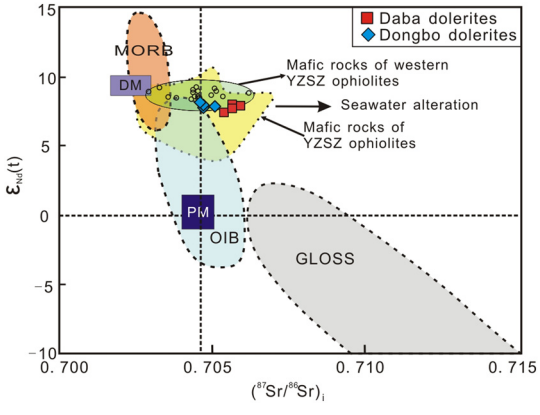


**Fig. 6.** Binary plot of $\varepsilon_{Nd}(t)$ vs. $^{87}Sr/^{86}Sr_{(i)}$ for the investigated dolerite intrusions. Data for mafic rocks from the YZSZ ophiolites, OIB, GLOSS and MORB are shown for comparison. Abbreviations (in alphabetical order): DM = depleted mantle; GLOSS = global subducted sediment; MORB = mid-ocean ridge basalt; OIB = ocean island basalt; PM = primitive mantle. Sources: Aitchison et al. (2000), Liu et al. (2018a), Miller et al. (2003), Wang et al. (2006), Xiong et al. (2016), Zhang et al. (2005), Zhang et al. (2016a, b) and Zheng et al. (2017).

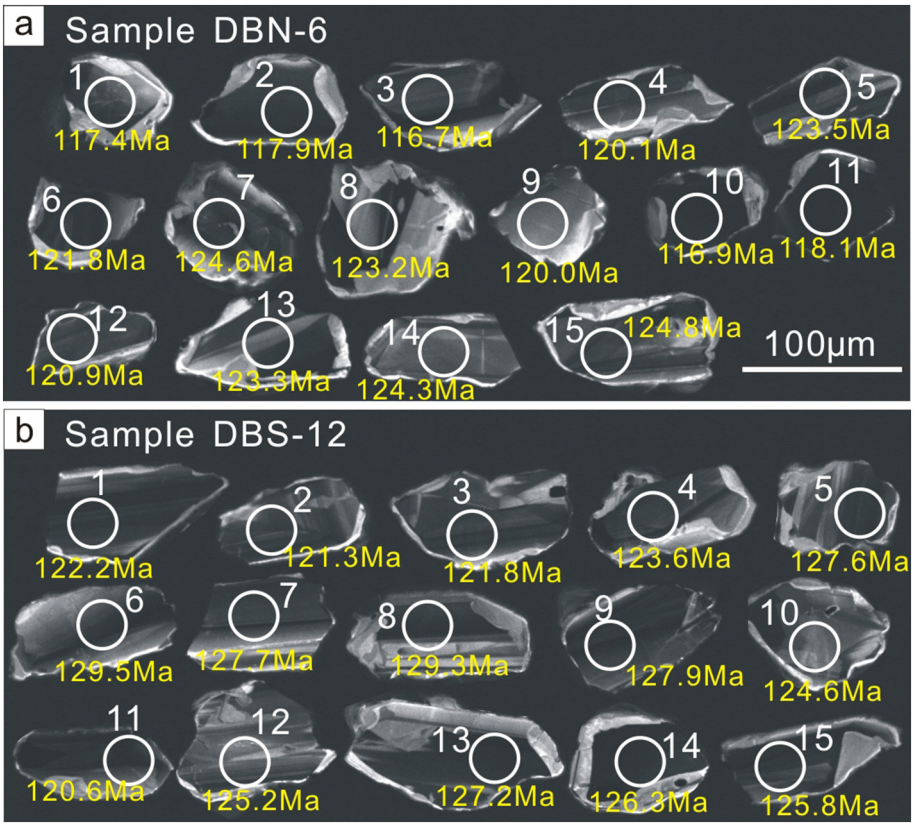


**Fig. 7.** Cathodoluminescence (CL) images and U—Pb crystallisation ages of (magmatic) zircons separated from the Daba (a) and Dongbo (b) dolerite dykes.

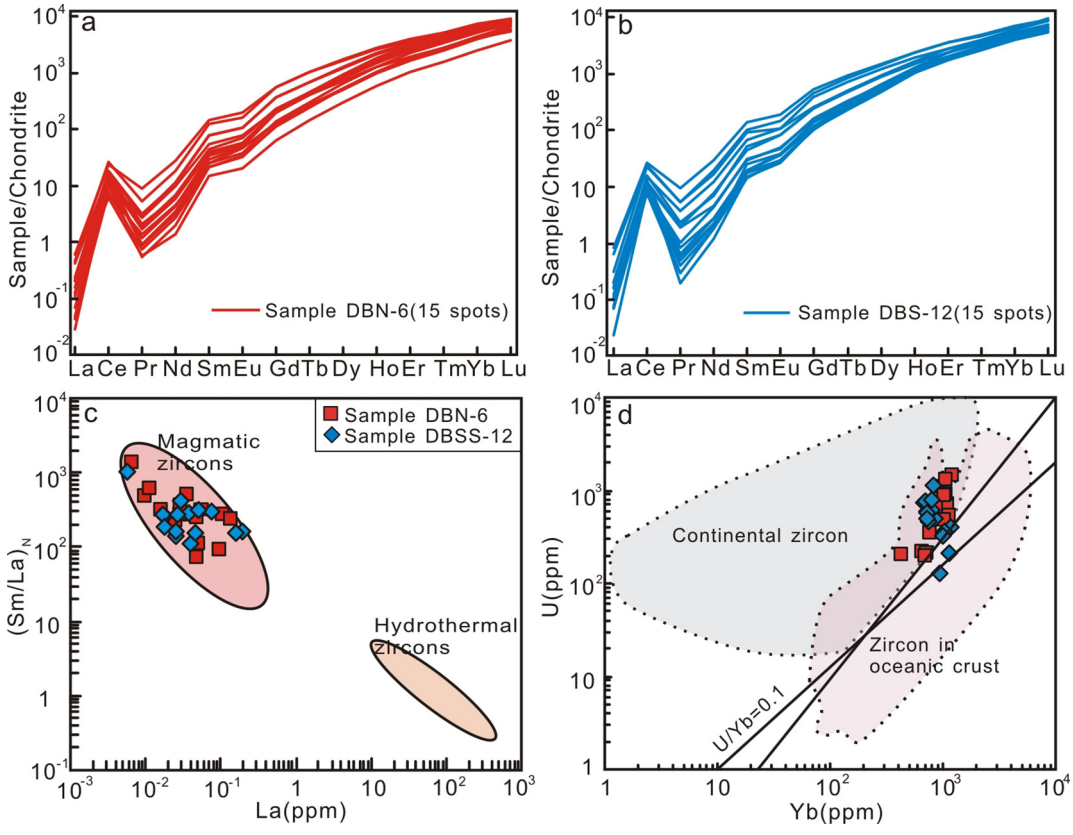


**Fig. 8.** Chondrite-normalised REE patterns for zircons separated from the Daba (a) and Dongbo (b) dolerite dykes. Discriminant diagrams of (c) $(Sm/La)_N$ vs. La (after Hoskin, 2005) and (d) U vs. Yb (after Grimes et al., 2007) for zircons separated from the investigated dolerite dykes.

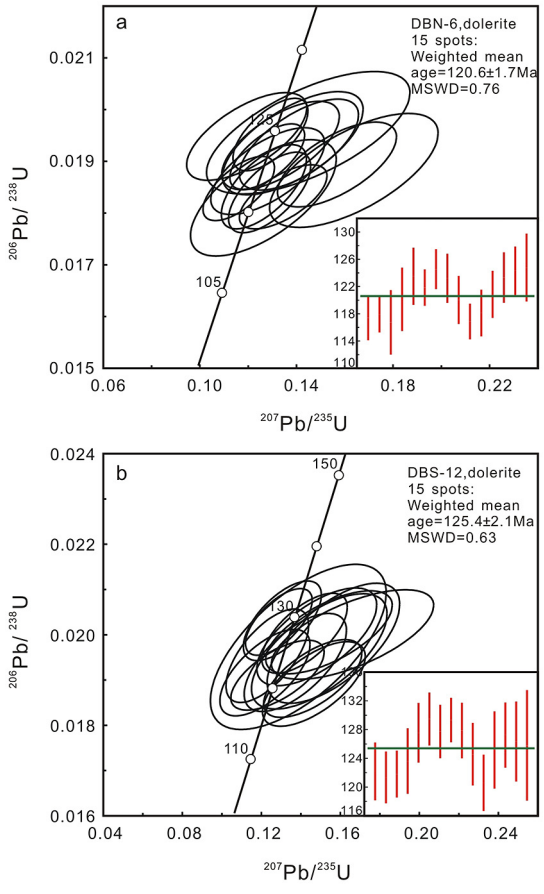


**Fig. 9.** Concordia curves of the U—Pb data of zircons separated from the Daba (a) and Dongbo (b) dolerite dykes.

the fields of volcanic-arc basalts and N-MORB lavas (Fig. 4c). However, on the discrimination diagram V vs. $Ti/10^3$ (Shervais, 1982), the Daba dolerite dykes (Ti/V = 16–27) straddle the boundaries between the fields of MORB and island arc tholeiite (IAT) lavas, whereas the Dongbo dolerite dykes (Ti/V = 27–38) plot in the field of lavas with a MORB-like geochemical affinity (Fig. 4d).

The total lanthanide contents of the Daba dolerite dykes are lower than those of the Dongbo dolerite intrusions (17.4–37.7 and 40.3–57.2 ppm, respectively). This indicates further that the investigated dolerite dykes represent a compositionally heterogeneous group of mafic intrusions.

Dolerite dykes from both the Daba and Dongbo peridotite massifs display chondrite-normalised lanthanide patterns that are characterised by slight depletions in the light lanthanides and nearly flat Tb to Lu segments (Fig. 5a). Some dolerite dykes from both massifs show weak negative Eu anomalies, implying the fractionation of plagioclase. The primitive mantle (PM)-normalised multi-element patterns of the dykes display variable depletions in Nb and marked enrichments in Ba and U (±Sr; Fig. 5b). The enrichments in Ba and U are probably due to secondary alteration (e.g., Saccani et al., 2017). Furthermore, a few dolerite samples from Dongbo show mild negative anomalies in Ti and Y (Fig. 5b). Overall, the geochemical signatures of the investigated rocks are comparable to those of other mafic dykes in the western YZSZ (Liu et al., 2018a).

### 5.3. Whole-rock Sr—Nd isotopes

The Rb contents of the Daba and Dongbo dolerite dykes show a negative correlation with their $Mg^{\#}$ values (data not shown). This implies that Rb was not mobilised during the post-magmatic stage. Consequently, the initial $^{87}Sr/^{86}Sr$ (hereafter $^{87}Sr/^{86}Sr_{(i)}$) ratios measured in the investigated mafic dykes are accurate.

The dolerite dykes from Daba have $^{87}Sr/^{86}Sr_{(i)}$ ratios of 0.707197 to 0.707879 and initial $^{143}Nd/^{144}Nd$ ratios (herein $^{143}Nd/^{144}Nd_{(i)}$) of 0.512861 to 0.512890. They also show high $\varepsilon_{Nd}(t)$ values of +7.4 to +7.9 (Table A2 in the supplementary file). The Sr—Nd isotopic characteristics of the dolerite dykes from Dongbo are similar to those of dolerite dykes from the Daba massif. In particular, they have $^{87}Sr/^{86}Sr_{(i)}$ ratios that range from 0.706108 to 0.706793, and $^{143}Nd/^{144}Nd_{(i)}$ ratios from 0.512874 to 0.512894. Furthermore, they show high $\varepsilon_{Nd}(t)$ values (+7.8 to +8.2; Table A2 in the supplementary file).

These Sr—Nd isotopic compositions are slightly lower than those reported for the MORB-like dolerite dykes in the nearby Purang massif ($^{143}Nd/^{144}Nd_{(t)}$ = 0.512904–0.512909, $\varepsilon_{Nd}(t)$ = +8.6 to +8.7; Liu et al., 2015a). They also differ significantly from the Sr—Nd isotopic compositions reported for the alkaline basalts in the Dongbo massif ($^{143}Nd/^{144}Nd_{(t)}$ = 0.512596–0.512630, $\varepsilon_{Nd}(t)$ = +2.6 to +3.3) and Purang massif ($^{143}Nd/^{144}Nd_{(t)}$ = 0.512777–0.512779, $\varepsilon_{Nd}(t)$ = +6.1 to +6.2; Liu et al., 2015a).

On the $\varepsilon_{Nd}(t)$ vs. $^{87}Sr/^{86}Sr_{(i)}$ binary diagram, the isotopic signatures of the investigated mafic dykes plot in the field of mafic rocks from the (western) YZSZ ophiolites (Fig. 6).

### 5.4. Zircon

#### 5.4.1. Microtexture and composition

The zircon grains separated from samples of the dolerite dykes in both study areas (samples DBN-6 and DBS-12) have similar microstructures and compositions. Under transmitted light the zircons are transparent with an average size of ~80 × 40 μm. They are mostly anhedral to subhedral and less frequently angular. In CL images, the zircons show weak to strong sector zoning parallel to external crystal faces, or irregular internal zoning (Fig. 7a, b). A few zircons with variably bright domains along their crystal boundaries were also observed in CL images (Fig. 7a, b). These bright areas may be due to the interaction of zircons with post-magmatic fluids. All the zircons are free of visible mineral inclusions and overgrowths; furthermore, they show no sign of magmatic resorption or detrital derivation, and have no inherited cores (Fig. 7a, b).

The zircons from the dolerite dykes show variable contents of U (DBN-6 = 195–1456 ppm, DBS-12 = 127–1167 ppm) and Th (DBN-6 = 102–2763 ppm, DBS-12 = 83.5–1684 ppm; Table A4–1 in the supplementary file). All these zircons have high Th/U ratios (DBN-6 = 0.5–1.9, DBS-12 = 0.4–1.5), as is typical of magmatic zircons (Hoskin and Schaltegger, 2003; Rubatto, 2002), and this is consistent with the *T* values obtained using the Ti-in-zircon thermometer of Cherniak and Watson (2007). The geothermometric calculations show that the zircons crystallised at high temperatures ($T_{DBN-6}$ = 652–747 °C, $T_{DBS-12}$ = 659–725 °C), thus ruling out any possibility that the zircons were derived from post-magmatic fluids.

The lanthanide contents of the zircons (Table A3 in the supplementary file) were normalised to the concentrations of lanthanides in chondrite (Sun and McDonough, 1989), and plotted on $\log_{10}$ vs. trace element (La to Lu) diagrams (Fig. 8a, b). The chondrite-normalised lanthanide profiles of zircons from both dolerite dyke samples (DBN-6 and DBS-12) show relatively steep positive slopes from La to Lu with positive Ce and Sm anomalies and weak negative Eu anomalies, indicating either crystallisation of zircon before plagioclase or crystallisation from a melt derived from a source that originally contained no plagioclase (Fig. 8a, b). The similarity in the multi-element lanthanide-patterns of zircons recovered from the Daba and Dongbo dolerite dykes implies that their lanthanide budgets were controlled by magmatic processes that affected each dolerite intrusion in a similar way. This is further corroborated by the high $(Sm/La)_N$ ratios for low La concentrations in all the zircons, which is indicative of a magmatic origin (Hoskin, 2005; Fig. 8c). On the U vs. Yb discrimination diagram

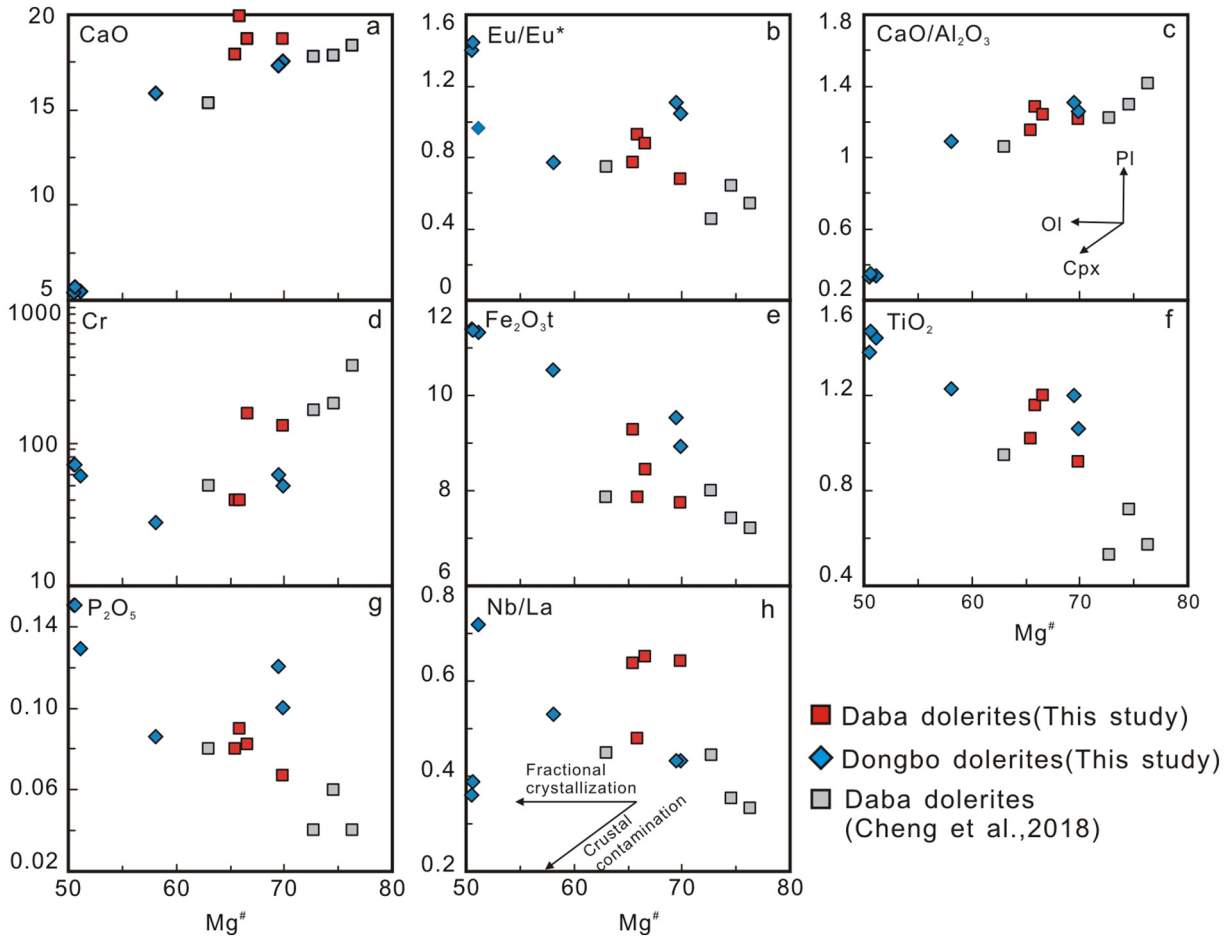


**Fig. 10.** (a-h) Plots of CaO, Eu/Eu*, $CaO/Al_2O_3$, Cr, $Fe_2O_3^t$, $TiO_2$, $P_2O_5$, Nb/La vs. Mg# for the Dongbo and Daba dolerite dykes.

(Grimes et al., 2007), zircons from the dolerite intrusions straddle the boundary between the continental zircon and ocean-crust zircon fields (Fig. 8d).

The zircon grains show analogous microstructural and compositional characteristics, even though they were recovered from different mafic dykes from distinct peridotite massifs. This probably indicates that the dolerite intrusions within the Daba and Dongbo peridotites share a common petrological history.

*5.4.2. U—Pb geochronology*

U—Pb ages were obtained from 15 spot analyses of zircons separated from each dolerite dyke sample (Table A4–1 in the supplementary file). On a $^{207}Pb/^{235}U$ vs. $^{206}Pb/^{238}U$ concordia diagram, the zircons from dolerite sample DBN-6 yield a weighted mean $^{206}Pb/^{238}U$ age of 121 ± 2 Ma (MSWD = 0.76; Fig. 9a), whereas those from dolerite specimen DBS-12 yield a weighted mean $^{206}Pb/^{238}U$ age of 125 ± 2 Ma (MSWD = 0.63; Fig. 9b). These data are near-concordant, probably due to Pb loss during later geological events (Dickin and Muller, 2005) or imprecise measuring of $^{207}Pb$ (Yuan et al., 2008). The data show no correlation between U—Pb ages and crystal morphology or internal microtextures of the investigated zircons.

Geochronological dating of zircons separated from pyroxenite and gabbro intrusions within the Dongbo mantle peridotites yielded somewhat older U—Pb ages (130.4 ± 0.5 and 128.5 ± 1.1 Ma, respectively; Xiong et al., 2011) than those of the zircons investigated here, but the U—Pb ages of zircons from the dolerite dykes of the Dongbo and Daba massifs are analogous to those of zircons recovered from the dolerite intrusions and gabbros of the nearby Purang massif (130 ± 3.0 Ma reported by Liu et al., 2011; 122.3 ± 2.4 Ma reported by Li et al., 2008), respectively.

## 6. Discussion

### *6.1. Potential effects of metasomatism, crustal assimilation and fractional crystallisation*

Various processes, including mantle metasomatism, crustal assimilation and magmatic differentiation, may significantly affect the original composition of a mafic rock (e.g., Saccani et al., 2014). Therefore, the impact of these processes on the geochemistry of the Daba and Dongbo dolerite dykes must be evaluated thoroughly before we can understand the compositional signatures of the mantle sources of their parental magmas.

Dolerite dykes from both massifs present no evidence of interaction with the mantle peridotites they intruded. In particular, they lack mantle-derived xenoliths or xenocrysts, and they have sharp contacts with their host harzburgites. These observations imply that the dyke-filling melts did not interact mechanically or physicochemically with the surrounding harzburgites or peridotites they encountered during ascent to shallow mantle levels. Furthermore, the investigated dolerite dykes lack high-*T* deformation fabrics, indicating that the emplacement of the mafic magma took place after the earlier ductile deformation of the mantle. Some dolerite dykes at Dongbo have chilled margins, which imply formation in a cold lithospheric environment that allowed for the rapid solidification of the magma (e.g., Xiong et al., 2016).

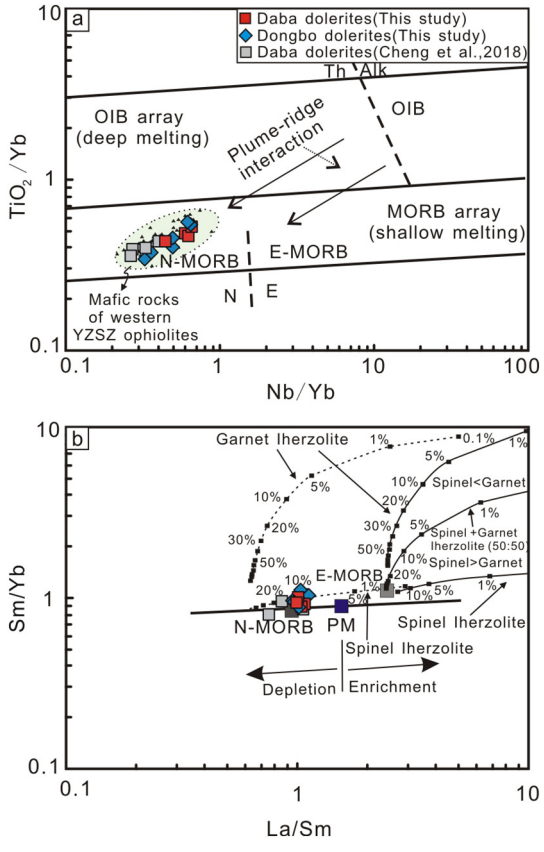


**Fig. 11.** a) $TiO_2$/Yb vs. Nb/Yb discrimination diagram (after Pearce, 2008) and b)Sm/Yb vs. La/Sm discrimination diagram (after Aldanmaz et al., 2000) for the Dongbo and Daba dolerite dykes. Melt curves (or lines) were obtained using the non-modal batch melting equations of Shaw (1970). Melt curves are drawn for spinel-lherzolite (with peridotite mode and melt mode of: $Ol_{0.53}$ + $Opx_{0.27}$ + $Cpx_{0.17}$ + $Sp_{0.03}$ and -$Ol_{0.06}$ + $Opx_{0.28}$ + $Cpx_{0.67}$ + $Sp_{0.11}$; respectively; Kinzler, 1997) and for garnet-lherzolite (with peridotite mode and melt mode of: $Ol_{0.60}$ + $Opx_{0.20}$ + $Cpx_{0.10}$ + $Gt_{0.10}$ and $Ol_{0.03}$ + $Opx_{0.16}$ + $Cpx_{0.88}$ + $Gt_{0.09}$, respectively; Walter, 1998). Mineral/matrix partition coefficients and DMM are from the compilation of McKenzie and O'Nions (1991, 1995); PM, N-MORB and E-MORB compositions are from Sun and McDonough (1989). The heavy line represents the mantle array defined using DMM and PM compositions. Dashed curves (or lines) are the melting trends for DMM. Thick marks on each curve (or line) correspond to degrees of partial melting for a given mantle source. Abbreviations (in alphabetical order): Alk = alkaline; E-MORB = enriched-type mid-ocean ridge basalt; OIB = ocean island basalt; N-MORB = normal-type mid-ocean ridge basalt; Th = tholeiitic.

The investigated dolerite dykes crop out as isolated intrusions that show no microtextural or compositional layering, and no "topographic" intrusional boundaries as in typical cumulate intrusives (e.g., Kapsiotis et al., 2018).They are found exclusively within the mantle sections of both investigated massifs, ruling out any possibility of interaction of the dyke-filling melts with crustal lithologies.

The low Cr contents of the Daba and Dongbo dolerite dykes (40–350 and 28–70 ppm, respectively; Table A1–1 in the supplementary file) imply that they were not derived from primitive magmas, which typically have Cr contents >400 ppm (Tatsumi and Eggins, 1995).The wide ranges in $Mg^{\#}$ values for the Daba and Dongbo mafic dykes (63.00–76.29 and 50.55–69.86, respectively; Table A1–1 in the supplementary file) indicate that they originated from variably fractionated melts. The near-positive correlation between CaO and $Mg^{\#}$, and the negative correlation between Eu/Eu* and $Mg^{\#}$ (Fig. 10a, b) reflect the fractional crystallisation of plagioclase. The positive correlation between $CaO/Al_2O_3$ and $Mg^{\#}$ (Fig. 10c), and the negative correlation between Cr and $Mg^{\#}$ (Fig. 10d) indicate the significant fractionation of clinopyroxene (e.g., Naumann and Geist, 1999). In addition, the negative correlations between $Fe_2O_3^t$, $TiO_2$, $P_2O_5$ and $Mg^{\#}$ (Fig. 10e–g) indicate negligible fractionation of Fe—Ti oxides and apatite from the dyke-filling melts. However, the weak negative correlation between Nb/La and $Mg^{\#}$ (Fig. 10h) cannot be the result of magma fractionation or contamination by crustal rocks (e.g., Liu et al., 2016), and it seems, therefore, that the trace element budgets of the dolerite dykes were not controlled by igneous processes and that they are probably close to the original values. For this reason, various trace element ratios (i.e., Zr/Y, Zr/Nb, Nb/Yb, Th/Yb, La/Sm and Sm/Yb) are used to infer the compositional characteristics of the mantle source(s) of the dyke-filling melts. This is because such ratios could only have been weakly affected by the fractional crystallisation of plagioclase and clinopyroxene (Saccani et al., 2014), and are therefore likely to represent the original elemental ratios in the inferred mantle source regions (Baker et al., 1997).

### 6.2. Mantle source characteristics and melting conditions

On the $TiO_2$/Yb vs. Nb/Yb discrimination diagram (Pearce, 2008), the dolerite dykes from the Daba and Dongbo massifs plot in the shallow melting array, showing analogous compositions to those of MORB-type tholeiites (Fig. 11a). This is in accordance with their chondrite-normalised lanthanide patterns (Fig. 5a), indicating derivation of the dyke-filling magmas from a depleted spinel-bearing mantle source (Aldanmaz et al., 2000; Saccani et al., 2008).

To assess the validity of this conclusion, $(Sm/Yb)_N$ values were calculated for the investigated dolerite intrusions. This ratio could be regarded as a potential indicator of the initiation of mantle melting in the stability field of garnet-bearing peridotite (Saccani et al., 2008). The range of $(Sm/Yb)_N$ values varies from 0.9 to 1.1 for the Daba dolerite dykes and from 1.0 to 1.2 for the Dongbo dolerite dykes, and these values are generally lower than those of basalts from the Alpine Corsican ophiolites (1.1–2.6), which are interpreted as the melting products of a depleted MORB-type peridotite source containing small amounts of garnet-bearing pyroxenite (Saccani et al., 2008). Consequently, the low $(Sm/Yb)_N$ ratios in the Daba and Dongbo dolerite dykes indicate that their parental melts were produced by partial melting of a spinel-bearing peridotite source.

Semi-quantitative lanthanide modelling can constrain the composition of the inferred mantle sources of the studied dolerite dykes. A non-modal, batch partial melting model (Aldanmaz et al., 2000) was used to estimate the source lithologies of the dyke-filling magmas. In this model, a garnet-dependent ratio (Sm/Yb) is plotted against an elemental ratio (La/Sm) that is not significantly affected by variations in the mantle source mineralogy, but which is largely controlled by fluctuations in the degree of partial melting (Aldanmaz et al., 2000). The applied model shows that the low Sm/Yb and La/Sm ratios of the Dongbo and Daba dolerite dykes can be reproduced by 10%–20% (cumulative) melting of a spinel-bearing lherzolite source (Kinzler, 1997; Fig. 11b).

### 6.3. Evidence for crustal inputs

Previous studies of the compositions of dolerite dykes in the Dongbo peridotite massif have shown that the mantle source of their parental melts was not significantly affected by crustal inputs (Liu et al., 2015a). The compositional data indicate that this is not entirely true. On the Th/Yb vs. Nb/Yb proxy diagram (Pearce, 2008; Fig. 12a), the dolerite dykes from both massifs plot above the MORB–OIB array, following a trend characterised by a general enrichment in Th. This implies that the mantle source of their parental magmas was affected, to some extent, by crustal inputs. Consequently, the question arises as to what kind of process caused the inferred crustal input. Was it lithospheric slab subduction, mafic melt–crust interaction (contamination), or deep recycling of crustal components within the upper mantle?

For each of these three processes, the precise compositional trajectory depends on variables that include the original magma composition,

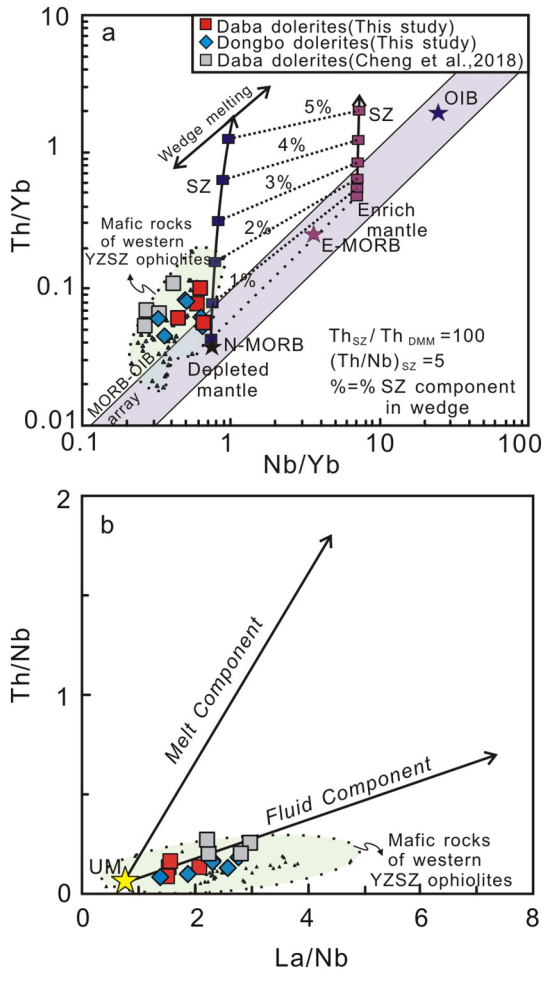


**Fig. 12.** a) Th/Yb vs. Nb/Yb diagram (after Pearce, 2008) and b) La/Nb vs. Th/Nb diagram (after Zamboni et al., 2016) for the investigated dolerite dykes. Abbreviations (in alphabetical order): E-MORB = enriched-type mid-ocean ridge basalt; OIB = ocean island basalt; N-MORB = normal-type mid-ocean ridge basalt; UM = Upper Mantle.

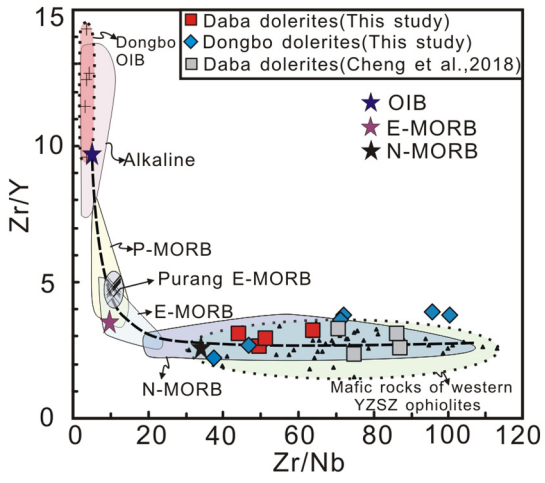


**Fig. 13.** Zr/Y vs. Zr/Nb diagram (after Saccani et al., 2013) for the investigated dolerite dykes. Stars indicate the compositions of modern OIB, E-MORB, and N-MORB (Sun and McDonough, 1989). The dashed line represents the mixing curve calculated using the OIB and N-MORB end-members. The compositional fields of theDongbo OIB (Liu et al., 2015a) are also shown. Abbreviations (in alphabetical order): OIB = ocean island basalt; N-MORB = normal-type mid-ocean ridge basalt.

contaminant compositions, and the relative proportions of magma and contaminant (Pearce, 2008). The data show that for the Daba and Dongbo dolerite dykes, a small input of subduction-related material (1%–2%) in the mantle source of their parental melts was responsible for an enrichment in Th (Fig. 12a). This is also supported by the following characteristics of the investigated dolerite intrusions: i) their negative anomalies in Nb (±Ti) in PM-normalised multi-element patterns are similar to those of tholeiitic magmas derived from arc-related settings (Fig. 5b), ii) the high average Zr/Nb ratio compared with that of the bulk crust (66.8 vs. 16.2; Rollinson et al., 2000), and iii) the compositions of the (magmatic) zircon grains they host, indicating crystallisation from magmas derived from melting of a mantle source that had been contaminated by subducted (crustal) material (Fig. 9b). Collectively, these findings indicate that the mantle source of the Dongbo and Daba dolerite dyke-filling melts was enriched by components released as a result of the melting of a downgoing oceanic lithospheric slab. This leads to the question as to what was the nature of the medium that modified the mantle source of the dyke-filling melts. Was it a melt or a fluid?

It is known that enrichment in fluid-mobile elements increases the La/Nb ratio of a mafic melt, whereas enrichment in melt-mobile elements results in magmas with high Th/Nb ratios (Pearce and Stern, 2006; Zamboni et al., 2016). The investigated dolerite dykes have high La/Nb ratios (1.4–3.0) and low Th/Nb ratios (0.08–0.27), indicating the involvement of slab-derived fluids rather than melts (Fig. 12b). This view is supported by the low Th/Nd ratios of the Dongbo and Daba dolerites (0.02–0.04), thus ruling out the involvement of sediment-derived melt components in the genesis of the parental magmas (Class et al., 2000). The investigated dolerite intrusions also display positive $\varepsilon_{Nd}(t)$ values and high $^{87}Sr/^{86}Sr_{(i)}$ ratios (Fig. 6), which points to a source region modified by hydrous fluids (Escrig et al., 2009). Collectively, these geochemical signatures indicate that the parental melts of the dolerite intrusions from both studied massifs were influenced by subduction-related aqueous fluids. These fluids aided the partial melting of a spinel-bearing mantle source region, causing fluid-mobile element enrichment in the resultant mafic melts.

The U—Pb crystallisation ages of magmatic zircons from the Daba and Dongbo dolerite dykes show that they were emplaced in the host harzburgites at 121 ± 2 and 125 ± 2 Ma, respectively (Fig. 9a, b). The genesis of the investigated dolerite dykes coincides with a known period of slab-derived mafic magmatism in South Tibet (~130–120 Ma; e.g., Dai et al., 2013; Griffin et al., 2016; Hébert et al., 2012; Wu et al., 2014; Xiong et al., 2016).

### 6.4. Tectonomagmatic implications

Various hypotheses have been proposed to explain the origin of the southwestern YZSZ ophiolites. They have been viewed as oceanic core complexes (OCC) exhumed along detachment faults (Liu et al., 2014) at a slow-spreading, possibly ultraslow-spreading, MOR (Miller et al., 2003). They have also been interpreted as products of decompressional mantle melting beneath a MOR followed by hydrous melting in a suprasubduction zone (SSZ) setting (Liu et al., 2010a; Su et al., 2015). Despite these contrasting scenarios, an increasing number of petrological studies have shown that the YZSZ mantle peridotites may not be genetically associated with their immediate crustal rocks (e.g., Gong et al., 2016; Griffin et al., 2016; McGowan et al., 2015; Xiong et al., 2016), and for the Dongbo and Purang peridotites in particular, it has been proposed that they represent old [sub-continental lithospheric (SCL)] mantle domains modified by ancient depletion events long before they were incorporated into the Neo-Tethyan Ocean (Gong et al., 2016).

The geological characteristics of the Daba and Dongbo massifs do not resemble those of typical SSZ-like ophiolites, and they are not consistent with any lithospheric or structural model of MOR-type ophiolites. The Dongbo massif has been interpreted as an Early Cretaceous lithospheric sequence from an ocean–continent transition (OCT) zone (Liu et al.,

2015a). This inference is supported by the observation that the Dongbo massif does not represent a typical Penrose-type ophiolite, but instead consists of upper mantle peridotites that are unconformably overlain by volcano–sedimentary rocks, and the field observations are in accordance with such an origin for the Dongbo massif (Fig. 2d–f). Furthermore, regional-scale exploration has shown that the tectonomagmatic structure of the Daba massif is analogous to that of the Dongbo massif (Fig. 2a–c), thus allowing us to also infer an origin from an OCT zone for the Daba ophiolite. However, there are several differences between the Daba and Dongbo massifs and other typical OCT massifs elsewhere, such as those cropping out along the Alpine–Apennine system (e.g., Lanzo). The most important of these include: i) the lack of plagioclase-bearing peridotites in the Daba and Dongbo ultramafic massifs, which contrasts with their common occurrence in typical OCT massifs (e.g., Müntener et al., 2010); and ii) the lack of spatially associated continental-derived blocks (extensional allochthons) such as those found in the Alpine–Apennine system ophiolites (e.g., Manatschal and Müntener, 2009). These differences could be explained by late-stage melt impregnation in the stability field of spinelperidotite, and by locating the investigated massifs more oceanwards relative to the ancient OCT zone. It is concluded, therefore, that a rifted continental margin setting can explain several geological and petrological characteristics of the investigated massifs. A similar setting has been proposed for the nearby Purang massif (Gong et al., 2016).

Thin (50–100 m) OIB-like lava layers occur in the extrusive sequence of the Dongbo massif, indicating a petrogenesis of this ophiolite that was influenced by plume-type magmatism at ~141 Ma (Liu et al., 2015a). Alkaline volcanism was followed by a younger phase (~129 ± 1.8 Ma) of MORB-type magmatism, as indicated by the geochemical signatures of the Dongbo isotropic gabbros (Liu et al., 2018b). The compositional and geochronological data also indicate that MORB-type magmatism postdated alkaline magmatism at Dongbo (125 ± 2 vs. 141 Ma). A distinction between these two types of magmatic activity is clear on a Zr/Y vs. Zr/Nb diagram (Sun and McDonough, 1989; Fig. 13). In this plot, the compositions of the alkaline lavas and tholeiitic intrusions from the Dongbo massif conform to the mixing curve computed using typical OIB and N-MORB end-member compositions (Sun and McDonough, 1989; Fig. 13). This implies that continental rifting and (subsequent) oceanic spreading were linked to the upwelling of a MORB-type asthenospheric source with decreasing plume-related components from deep to shallow mantle levels over time (e.g., Saccani et al., 2014). The absence of alkaline magmatism in the Daba area is consistent with this petrogenetic evolution.

Furthermore, the geochemical and isotopic signatures of the Daba and Dongbo dolerite dykes show that they were derived from the melting of a spinel-bearing mantle source region with minor inputs of subduction-derived fluids during the Early Cretaceous. This is most likely to have occurred during a stage of mantle melting in the wedge above a subducted oceanic lithospheric slab (Dai et al., 2013; Reagan et al., 2010). It is concluded, therefore, that the Daba and Dongbo dolerite intrusions were formed in an arc environment that was extending due to the rapid rollback of the descending Neo-Tethyan lithospheric slab during subduction initiation (~130–120 Ma; e.g., Maffione et al., 2015; Xiong et al., 2016; Zheng et al., 2017). The U—Pb zircon ages (127–124 Ma) and compositions of dolerite intrusions from the nearby Xigaze ophiolite (central-western YZSZ; Dai et al., 2013) are similar to those of the Dongbo and Daba dolerite dykes. The genesis of the Xigaze mafic intrusions has also been interpreted in terms of oceanic seafloor spreading in a forearc setting as a result of rapid slab rollback during subduction initiation between 130 and 120 Ma (Dai et al., 2013).

According to a recent model of the petrogenesis of the southwestern YSZS peridotites, arc-related metasomatism occurred only before their incorporation in a Neo-Tethyan oceanic basin (Gong et al., 2016). Here, it is argued that subduction-related phenomena also occurred after the accretion of those peridotites below a marginal basin (Liu et al., 2010a, 2012; Su et al., 2015). Moreover, it has been proposed that mafic intrusions within the southwestern YSZS peridotites lack evidence of contamination due to reaction with subducted lithospheric material, which would imply that they originated from the melting of a pure MORB-type peridotite source at shallow mantle depths. The compositional and geochronological findings are not incompatible with this idea. Furthermore, the present data indicate that the parental magmas of the investigated dolerites were generated by the melting of a fertile mantle source that had been weakly modified by fluids derived from the sedimentary cover of a downgoing lithospheric slab, when subduction was initiated adjacent to a rifted continental margin at ~130–120 Ma.

## 7. Conclusions

1. Magmatic zircons from dolerite dykes within the ophiolitic Daba and Dongbo peridotite massifs of the southwest Yarlung–Zangbo Suture Zone in SW Tibet yield U—Pb ages of 121 ± 2 and 125 ± 2 Ma, respectively.
2. The dolerite dykes show N-MORB-like lanthanide patterns with negative Nb anomalies, high $\varepsilon_{Nd}(t)$ values (+7.4 and + 8.2), and high values of $^{87}Sr/^{86}Sr_{(i)}$ (0.706108–0.707879).
3. Petrogenetic modelling shows that the parental magmas of the dykes were derived by 10%–20% (cumulative) melting of a spinel-bearing mantle source that had been modified by minor subduction-related inputs.
4. A tectonomagmatic model involving continental rifting and subsequent oceanic floor spreading, followed by the initiation of subduction adjacent to a passive margin, can best explain the geochemical and isotopic signatures of the dolerite intrusions within the Daba and Dongbo peridotites.

## Acknowledgments

We would like to express our gratitude to Prof. Guoqing Zhou for his analytical assistance and Dr. YunZhong, Dr.Zhengxin Yin and Prof. Wei Huang for their guidance during the field work. Prof. Liang Qi and Xianglin Tu are also greatly thanked for their help at the stage of the isotopic analyses of our samples. Special thanks are due to Prof. Andrew Kerr, Editor-in-Chief of Lithos, for his constructive feedback and editorial comments. The valuable comments and suggestions of two anonymous reviewers also helped us greatly improve our paper. This research was funded by the National Natural Science Foundation of China (Nos. 41402065, 41802001, 41472054 and 41602231), the Natural Science Foundation of Guangdong Province (Nos. 2017A030310395, 2018A030310303 and 2018B030311030) and the Natural Science Innovation Foundation of Department of Education of Guangdong Province (2016KTSCX001).

## Appendix A. Supplementary data

Supplementary data to this article can be found online at https://doi.org/10.1016/j.lithos.2018.10.023.

## References

Aitchison, J.C., Badengzhu, Davis, A.M., Liu, J., Luo, H., Malpas, J.G., McDermid, I.R.C., Wu, H., Ziabrev, S.V., Zhou, M., 2000. Remnants of a cretaceous intra-oceanic subduction system within the Yarlung-Zangbo suture (southern Tibet). Earth Planet. Sci. Lett. 183, 231–244.

Aldanmaz, E., Pearce, J.A., Thirlwall, M.F., Mitchell, J.G., 2000. Petrogenetic evolution of late Cenozoic, post-collision volcanism in western Anatolia, Turkey. J. Volcanol. Geotherm. Res. 102 (1), 67–95.

Baker, J.A., Menzies, M.A., Thirlwall, M.F., Macpherson, C.G., 1997. Petrogenesis of quaternary intraplate volcanism, Sana'a, Yemen: implications for plume-lithosphere interaction and polybaric melt hybridization. J. Petrol. 38 (10), 1359–1390.

Bao, P.S., Su, L., Wang, J., Zai, Q.G., 2015. Yarlung Zangbo River Ophiolite. Geological Publishing House, Beijing.

Bédard, É., Hébert, R., Guilmette, C., Lesage, G., Wang, C.S., Dostal, J., 2009. Petrology and geochemistry of the Saga and Sangsang ophiolitic massifs, Yarlung Zangbo Suture Zone, Southern Tibet: evidence for an arc-back-arc origin. Lithos 113 (1), 48–67.
Bézard, R., Hébert, R., Wang, C., Dostal, J., Dai, J., Zhong, H., 2011. Petrology and geochemistry of the Xiugugabu ophiolitic massif, western Yarlung Zangbo suture zone, Tibet. Lithos 125, 347–367.
Black, L.P., Kamo, S.L., Allen, C.M., Davis, D.W., Aleinikoff, J.N., Valley, J.W., Mundil, R., Campbell, I.H., Korsch, R.J., Williams, I.S., Foudoulis, C., 2004. Improved $^{206}Pb/^{238}U$ microprobe geochronology by monitoring of a trace-element-related matrix effect; SHRIMP, ID-TIMS, ELA-ICP-MS and oxygen isotope documentation for a series of zircon standards. Chem. Geol. 205 (1), 115–140.
Class, C., Miller, D.M., Goldstein, S.L., Langmuir, C.H., 2000. Distinguishing melt and fluid subduction components in Umnak Volcanics,Aleutian Arc, Geochem. Geophys. Geosyst. 1(6), 1004, doi:https://doi.org/10.1029/1999GC000010.
Coleman, R.G., 1977. Ophiolites: Ancient Oceanic Lithosphere? Springer, Berlin
Chan, G.H.N., Aitchison, J.C., Crowley, Q.G., Horstwood, M.S.A., Searle, M.P., Parrish, R.R., Chan, J.S.L., 2015. U-Pb zircon ages for Yarlung Tsangpo suture zone ophiolites, South-Western Tibet and their tectonic implications. Gondwana Res. 27 (2), 719–732.
Cheng, C., Xia, B., Zheng, H., Yuan, Y.J., Yin, Z.X., Lu, Y., Xu, C., Zhang, X., 2018. Chronology, Geochemistry and Tectonic Significance of Daba Ophiolites in theWestern Segment of the Yarlung Zangbo Suture Zone,Tibet. Earth Sci. 43 (4), 975–990 (in Chinese with English abstract).
Dai, J.G., Wang, C.S., Polat, A., Santosh, M., Li, Y.L., Ge, Y.K., 2013. Rapid forearc spreading between 130 and 120 Ma: evidence from geochronology and geochemistry of the Xigaze ophiolite, southern Tibet. Lithos 172–173 (4), 1–16.
Dickin, A.P., Muller, R., 2005. Radiogenic Isotope Geology: Radiogenic Isotope Geology. Cambridge University Press, Cambridge.
Dilek, Y., Furnes, H., 2011. Ophiolite genesis and global tectonics: geochemical and tectonic fingerprinting of ancient oceanic lithosphere. Geol. Soc. Am. Bull. 123, 387–411.
Dilek, Y., Furnes, H., 2014. Ophiolites and their Origins. Elements 10 (2), 93–100.
Dupuis, C., Hébert, R., Dubois-Côté, V., Wang, C.S., Li, Y.L., Li, Z.J., 2005. Petrology and geochemistry of mafic rocks from melange and flysch units adjacent to the Yarlung Zangbo Suture Zone, southern Tibet. Chem. Geol. 214 (3), 287–308.
Escrig, S., Bézos, A., Goldstein, S.L., Langmuir, C.H., Michael, P.J., 2009. Mantle source variations beneath the Eastern Lau spreading center and the nature of subduction components in the Lau basin-Tonga arc system. Geochem. Geophys. Geosyst. 10 (4), 115–123.
Gass, I.G., Ries, A.C., Shackleton, R.M., Smewing, J.D., 1990. Tectonics, Geochronology and Geochemistry of the Precambrian Rocks of Oman. 49(1). Geological Society London Special Publications, pp. 585–599.
Girardeau, J., Mercier, J.C., 1988. Petrology and texture of the ultramafic rocks of the Xigaze ophiolite (Tibet): constraints for mantle structure beneath slow spreading ridges. Tectonophysics 147 (1), 33–58.
Girardeau, J., Mercier, J.C., Yougong, Z., 1985. Origin of the Xigaze ophiolite, Yarlung Zangbo suture zone, southern Tibet. Tectonophysics 119 (1), 407–433.
Gong, X., Shi, R.D., Griffin, W.L., Huang, Q.S., Xiong, Q., Chen, S.S., Zhang, M., O'Reilly, S.Y., 2016. Recycling of ancient subduction-modified mantle domains in the Purang ophiolite (southwestern Tibet). Lithos 262, 11–26.
Grimes, C.B., John, B.E., Kelemen, P.B., Mazdab, F.K., Wooden, J.L., Cheadle, M.J., Hanghøj, K., Schwartz, J.J., 2007. Trace element chemistry of zircons from oceanic crust: a method for distinguishing detrital zircon provenance. Geology 35 (7), 643–646.
Griffin, W.L., Afonso, J.C., Belousova, E.A., Gain, S.E., Gong, X.H., González-Jiménez, J.M., Howell, D., Huang, J.X., McGowan, N., Pearson, N.J., Satsukawa, T., Shi, R., Williams, P., Xiong, Q., Yang, J.S., Zhang, M., O'Reilly, S.Y., 2016. Mantle recycling: transition zone metamorphism of Tibetan ophiolitic peridotites and its tectonic implications. J. Petrol. 57(4), 655–684.
Harrison, T.M., Yin, A., Grove, M., Lovera, O.M., Ryerson, F.J., Zhou, X., 2000. The Zedong Window: a record of superposed Tertiary convergence in southeastern Tibet. J. Geophys. Res. Solid Earth 105 (B8), 19211–19230.
He, J., Li, Y.L., Wang, C.S., Dilek, Y., Wei, Y.S., Chen, X., Hou, Y.L., Zhou, A., 2016. Plume proximal mid-ocean ridge origin of Zhongba mafic rocks in the western Yarlung Zangbo Suture Zone, Southern Tibet. J. Asian Earth Sci. 121, 34–55.
Hébert, R., Bezard, R., Guilmette, C., Dostal, J., Wang, C.S., Liu, Z.F., 2012. The Indus-Yarlung Zangbo ophiolites from Nanga Parbat to Namche Barwa syntaxes, southern Tibet: first synthesis of petrology, geochemistry, and geochronology with incidences on geodynamic reconstructions of Neo-Tethys. Gondwana Res. 22 (2), 377–397.
Hoskin, P.W.O., 2005. Trace-element composition of hydrothermal zircon and the alteration of hadean zircon from the jack hills, Australia. Geochim. Cosmochim. Acta 69 (3), 637–648.
Hoskin, P.O.W., Schaltegger, U., 2003. The composition of zircon and igneous and metamorphic petrogenesis. Rev. Mineral. Geochem. 53 (1), 27–62.
Hu, X.M., Garzanti, E., Wang, J., Huang, W., An, W., Webb, A., 2016. The timing of India-Asia collision onset-Facts, theories, controversies. Earth Sci. Rev. 160, 264–299.
Ji, W.Q., Wu, F.Y., Chung, S.L., Li, J.X., Liu, C.Z., 2009. Zircon U-Pb geochronology and Hf isotopic constraints on petrogenesis of the Gangdese batholith, southern Tibet. Chem. Geol. 262 (3), 229–245.
Kinzler, R.J., 1997. Melting of mantle peridotite at pressures approaching the spinel to garnet transition: application to mid-ocean ridge basalt petrogenesis. J. Geophys. Res. Solid Earth 102 (B1), 853–874.
Kapsiotis, A., Rassios, A.E., Uysal, I., Grieco, G., Akmaz, R.M., Saka, S., Bussolesi, M., 2018. Compositional fingerprints of chromian spinel from the refractory chrome ores of Metalleion, Othris (Greece): Implications for metallogeny and deformation of chromitites within a "hot" oceanic fault zone. J. Geochem. Explor. 185, 14–32.
Lebas, M.J., Le Maitre, R.W., Streckeisen, A., Zanettin, B., 1986. A chemical classificationof volcanic rocks based on the total alkali-silica diagram. J. Petrol. 27 (3), 745–750.
Li, J.F., Xia, B., Liu, L.W., Xu, L.F., He, G.S., Wang, H., Zhang, Y.Q., Yang, Z.Q., 2008. SHRIMP U-Pb zircon dating of diabase in the Langa Co ophiolite, Purang, Tibet, China, and its geological significance. Geol. Bull. China 27 (10), 1739–1743 (in Chinese with English abstract).
Li, X.H., Liu, Y., Li, Q.L., Guo, C.H., Chamberlain, K.R., 2009. Precise determination of Phanerozoic zircon Pb/Pb age by multicollector SIMS without external standardization. Geochem. Geophys. Geosyst. 10, Q04010.
Liu, C.Z., Wu, F.Y., Chu, Z.Y., Ji, W.Q., Yu, L.J., Li, J.L., 2012. Preservation of ancient Os isotope signatures in the Yungbwa ophiolite (southwestern Tibet) after subduction modification. J. Asian Earth Sci. 53 (3), 38–50.
Liu, C.Z., Wu, F.Y., Wilde, S.A., Yu, L.J., Li, J.L., 2010a. Anorthitic plagioclase and pargasitic amphibole in mantle peridotites from the Yungbwa ophiolite (southwestern Tibetan Plateau) formed by hydrous melt metasomatism. Lithos 114 (3–4), 413–422.
Liu, C.Z., Zhang, C., Yang, L.Y., Zhang, L.L., Ji, W.Q., Wu, F.Y., 2014. Formation of gabbronorites in the Purang ophiolite (SW Tibet) through melting of hydrothermally altered mantle along a detachment fault. Lithos 205 (10), 127–141.
Liu, F., Yang, J.S., Dilek, Y., Xu, Z.Q., Xu, X.Z., Liang, F.H., Chen, S.Y., Lian, D.Y., 2015a. Geochronology and geochemistry of basaltic lavas in the Dongbo and Purang ophiolites of the Yarlung-Zangbo Suture zone: Plume-influenced continental margin-type oceanic lithosphere in southern Tibet. Gondwana Res. 27 (2), 701–718.
Liu, F., Yang, J.S., Lian, D.Y., Zhao, H., Zhang, L., Zhang, L., Huang, J., 2015b. Genesis and characteristics of the western part of the Yarlung Zangboophiolites, Tibet. Acta Petrol. Sin. 31 (s2), 3609–3628 (in Chinese with English abstract).
Liu, F., Dilek, Y., Xie, Y., Yang, J.S., Lian, D.Y., 2018a. Melt evolution of upper mantle peridotites and mafic dykes in the northern ophiolite belt of the western Yarlug Zangbo Suture Zone (southern Tibet). Lithosphere 10 (1), 109–132.
Liu, F., Lian, D.Y., Niu, X.L., Zhao, H., Feng, G.Y., Yang, J.S., 2018b. Dongbo MORB-Type Isotropic Gabbro Emplaced as an Oceanic Core Complex in Western Yarlung Zangbo Suture Zone,Tibet. Earth Sci. 43 (4), 952–974 (in Chinese with English abstract).
Liu, T., Wu, F.Y., Zhang, L.L., Zhai, Q.G., Liu, C.Z., Ji, W.B., Zhang, C., Xu, Y., 2016. Zircon U-Pb geochronological constraints on rapid exhumation of the mantle peridotite of the Xigaze ophiolite, southern Tibet. Chem. Geol. 443, 67–86.
Liu, Y.S., Gao, S., Hu, Z.C., Gao, C.G., Zong, K.Q., Wang, D.B., 2010b. Continental and oceanic crust recycling-induced melt-peridotite interactions in the Trans-North China Orogen: U-Pb dating, Hf isotopes and trace elements in zircons from mantle xenoliths. J. Petrol. 51 (1–2), 537–571.
Liu, Z., Li, Y., Xiong, F.H., Wu, D., Liu, F., 2011. Petrology and geochronology of MOR gabbro in the Purang ophiolite of western Tibet, China. Acta Petrol. Sin. 27 (11), 3169–3279 (in Chinese with English abstract).
Ludwig, K.R., 2003. ISOPLOT 3.00: a Geochronological Toolkit for Microsoft Excel. Special Publication no. 4. Berkeley Geochronology Center, Berkeley.
MacDonald, G.A., Katsura, I., 1964. Chemical composition of Hawaiian Lavas. J. Petrol. 5, 82–133.
Manatschal, G., Müntener, O., 2009. A type sequence across an ancient magma-poor ocean continent transition: the example of the western Alpine Tethys ophiolites. Tectonophysics 473, 4–19.
McGowan, N., Griffin, W.L., Gonzalez-Jimenez, J.M., Belousova, E.A., Afonso, J.C., Shi, R., McCammon, C., Pearson, N.J., O'Reilly, S.Y., 2015. Tibetan chromitites: excavating the slab graveyard. Geology 43 (2), 179–182.
McKenzie, D., O'Nions, R.K., 1991. Partial melt distributions from inversion of rare earth element concentrations. J. Petrol. 32 (6), 1021–1091.
McKenzie, D.P., O'Nions, R.K., 1995. The source regions of Ocean Island Basalts. J. Petrol. 36, 133–159.
Meschede, M., 1986. A method of discriminating between different types of mid-ocean ridge basalts and continental tholeiites with the Nb-Zr-Y diagram. Chem. Geol. 56 (3), 207–218.
Miller, C., Thöni, M., Framk, W., Schuster, R., Melcher, F., Meisel, T., Zanetti, A., 2003. Geochemistry of tectonomagmatic affinity of the Yungbwa ophiolite, SW Tibet. Lithos 66 (3), 155–172.
Moghadam, H.S., Stern, R.J., 2011. Late cretaceous forearc ophiolites of Iran. Island Arc 20, 1–4.
Müntener, O., Manatschal, G., Desmurs, L., Pettke, T., 2010. Plagioclase peridotites in ocean-continent transitions: refertilized mantle domains generated by melt stagnationin the shallow mantle lithosphere. J. Petrol. 51, 255–294.
Naumann, T.R., Geist, D.J., 1999. Generation of alkalic basalt by crystal fractionation oftholeiitic magma. Geology 27, 423–426.
Nicolas, A., Girardeau, J., Marcoux, J., Dupré, B., Wang, X., Cao, Y., Zheng, H., Xiao, X., 1981. The Xigaze ophiolite (Tibet): a peculiar oceanic lithosphere. Nature 294, 414–417.
Niu, X.L., Yang, J.S., Dilek, Y., Xu, J.F., Li, J., Chen, S.Y., Feng, G.Y., Liu, F., Xiong, F.H., Liu, Z., 2015. Petrological and Os isotopic constraints on the origin of the Dongbo peridotite massif, Yarlung Zangbo suture zone, western Tibet. J. Asian Earth Sci. 110, 72–84.
Pan, G.T., Ding, J., Yao, D.S., Wang, L.Q., 2004. Guidebook of 1:1,500,000 Geologic Map of the Qinghai-Xizang (Tibet) Plateau and Adjacent Areas. Chengdu Cartographic Publishing House, Chengdu (in Chinese).
Pearce, J.A., 2008. Geochemical fingerprinting of oceanic basalts with applications to ophiolite classification and the search for Archean oceanic crust. Lithos 100 (1), 14–48.
Pearce, J.A., Deng, W.M., 1988. The Ophiolites of the Tibetan Geotraverses, Lhasa to Golmud (1985) and Lhasa to Kathmandu (1986). 327(1594). Philosophical transactions of the Royal Society a: Mathematical, Phys Eng Sci, pp. 215–238.
Pearce, J.A., Stern, R.J., 2006. Origin of Back-Arc Basin Magmas: Trace Element and Isotope Perspectives. AGU Geophysical monograph series 166 pp. 63–86.
Reagan, M.K., Ishizuka, O., Stern, R.J., Kelley, K.A., Ohara, Y., Blichert-Toft, J., Bloomer, S.H., Cash, J., Fryer, P., Hanan, B.B., Hickey-Vargas, R., Ishii, T., Kimura, J.I., Peate, D.W., Rowe, M., Woods, M., 2010. Fore-arc basalts and subduction initiation in the Izu-Bonin-Mariana system. Geochem. Geophys. Geosyst. 11 (3), 1–17.

Rollinson, H.R., Yang, X.M., Yang, X.Y., Chen, S.X., 2000. Lithogeochemistry. University of Science and Technology of China Press, Hefei, pp. 1–275 (in Chinese).
Rubatto, D., 2002. Zircon trace element geochemistry: partitioning with garnet and the link between U–Pb ages and metamorphism. Chem. Geol. 184 (1), 123–138.
Saccani, E., Principi, G., Garfagnoli, F., Menna, F., 2008. Corsica ophiolites: geochemistry and petrogenesis of basaltic and metabasaltic rocks. Ofioliti 33 (2), 187–207.
Saccani, E., Allahyari, K., Beccaluva, L., Bianchini, G., 2013. Geochemistry and petrology of the Kermanshah ophiolite (Iran): implication for the interaction between passive rifting, oceanic accretion, and OIB-type components in the Southern Neo-Tethys Ocean. Gondwana Res. 24 (1), 392–411.
Saccani, E., Allahyari, K., Rahimzadeh, B., 2014. Petrology and geochemistry of mafic magmatic rocks from the Sarve-Abad ophiolites (Kurdistan region, Iran): evidence for interaction between MORB-type asthenosphere and OIB-type components in the southern Neo-Tethys Ocean. Tectonophysics 621, 132–147.
Saccani, E., Delavari, M., Dolati, A., Marroni, M., Pandolfi, L., Chiari, M., Barbero, E., 2017. New insights into the geodynamics of Neo-Tethys in the Makran area: evidence from age and petrology of ophiolites from the Coloured Mélange complex (SE Iran). Gondwana Res. 62, 306–327.
Shaw, D.M., 1970. Trace element fractionation during anatexis. Geochim. Cosmochim. Acta 34, 237–243.
Shervais, J.W., 1982. Ti-V plots and the petrogenesis of modern and ophiolitic lavas. Earth Planet. Sci. Lett. 59 (1), 101–118.
Stern, R.J., Bloomer, S.H., 1992. Subduction zone infancy: examples from the Eocene Izu-Bonin-Mariana and Jurassic California arcs. Geol. Soc. Am. Bull. 104 (12), 1621–1636.
Su, B.X., Teng, F.Z., Hu, Y., Shi, R.D., Zhou, M.F., Zhu, B., Liu, F., Gong, X.H., Huang, Q.S., Xiao, Y., Chen, C., He, Y.S., 2015. Iron and magnesium isotope fractionation in oceanic lithosphere and sub-arc mantle: perspectives from ophiolites. Earth Planet. Sci. Lett. 430, 523–532.
Sun, S.S., McDonough, W.F., 1989. Chemical and Isotopic Systematics of Oceanic Basalts: Implications for Mantle Composition and Processes. 42(1). Geological Society London Special Publications, pp. 313–345.
Tatsumi, Y., Eggins, S.M., 1995. Subduction Zone Magmatism. Blackwell Science.
Cherniak, D.J., Watson, E.B., 2007. Ti diffusion in zircon. Chem. Geol. 242 (3–4), 470–483.
Walter, M.J., 1998. Melting of garnet peridotite and the origin of komatiite and depleted lithosphere. J. Petrol. 39 (1), 29–60.
Wang, C.S., Liu, Z.F., Hébert, R., 2000. The Yarlung-Zangbo paleo-ophiolite, southern Tibet: implications for the dynamic evolution of the Yarlung-Zangbo Suture Zone. J. Asian Earth Sci. 18 (6), 651–661.
Wang, R., Xia, B., Hu, J.R., Zhou, G.Q., Wei, D.L., Wang, X.B., 2006. Geochemistry of oceanic island diabase from ophiolitic melange zone in Renbu area: implications for hotspot within Tethys in southern Xizang (Tibet). Geochimica 35 (1), 41–54 (in Chinese with English abstract).
Winchester, J.A., Floyd, P.A., 1977. Geochemical discrimination of different magma series and their differentiation products using immobile elements. Chem. Geol. 20 (4), 325–343.
Wu, F.Y., Liu, C.Z., Zhang, L.L., Zhang, C., Wang, J.G., Ji, W.Q., Liu, X.C., 2014. Yarlung Zangbo ophiolite: a critical updated view. Acta Petrol. Sin. 30 (2), 293–325 (in Chinese with English abstract).
Xia, B., Chen, G.W., Wang, R., Wang, Q., 2008. Seamount volcanism associated with the Xigaze ophiolite, Southern Tibet. J. Asian Earth Sci. 32, 396–405.
Xiong, F.H., Yang, J.S., Liang, F.H., Ba, D.Z., Zhang, J., Xu, X.Z., Li, Y., Liu, Z., 2011. Zircon U-Pb ages of the Dongbo ophiolite in the western Yarlung Zangbo suture zone and their geological significance. Acta Petrol. Sin. 27 (11), 3223–3238 (in Chinese with English abstract).
Xiong, Q., Griffin, W.L., Zheng, J.P., O'Reilly, S.Y., Pearson, N.J., Xu, B., Belousova, E.A., 2016. Southward trench migration at 130–120 Ma caused accretion of the Neo-Tethyan forearc lithosphere in Tibetan ophiolites. Earth Planet. Sci. Lett. 438, 57–65.
Xiong, F.H., Yang, J.S., Robinson, P.T., Xu, X.Z., Liu, Z., Zhou, W.D., Feng, G.Y., Xu, J.F., Li, J., Niu, X.L., 2017. High-Al and high-Cr podiform chromitites from the western Yarlung-Zangbo suture zone, Tibet: implications from mineralogy and geochemistry of chromian spinel, and platinum-group elements. Ore Geol. Rev. 80, 1020–1041.
Xu, Z., Dilek, Y., Yang, J., Liang, F., Liu, F., Ba, D., Cai, Z., Li, G., Dong, H., Ji, S., 2015. Crustal structure of the Indus-Tsangpo suture zone and its ophiolites in southern Tibet. Gondwana Res. 27, 507–524.
Yang, J.H., Wu, F.Y., Shao, J.A., Wilde, S.A., Xie, L.W., Liu, X.M., 2006. Constraints on the timing of uplift of the YanshanFold and Thrust Belt, North China. Earth Planet. Sci. Lett. 246, 336–352.
Yang, J.S., Xiong, F.H., Guo, G.L., Liu, F., Liang, F.H., Chen, S.Y., Li, Z.L., Zhang, L.W., 2011. The Dongbo ultramafic massif: a mantle peridotite in the western part of the Yarlung Zangbo suture zone, Tibet, with excellent prospects for a major chromite deposit. Acta Petrol. Sin. 27 (11), 3207–3222 (in Chinese with English abstract).
Yin, A., Harrison, T.M., 2000. Geologic evolution of the Himalayan-Tibetan orogen. Ann. Rev. Earth Planet. Sci. Lett. 28, 211–280.
Yuan, H.L., Gao, S., Dai, M.N., Zong, C.L., Günther, D., Fontaine, G.H., Liu, X.M., Diwu, C.R., 2008. Simultaneous determinations of U-Pb age, Hf isotopes and trace element compositions of zircon by excimer laser ablation quadrupole and multiple collector ICP-MS. Chem. Geol. 247 (1), 100–118.
Zamboni, D., Gazel, E., Ryan, J.G., Cannatelli, C., Lucchi, F., Atlas, Z.D., Trela, J., Mazza, S.E., De Vivo, B., 2016. Contrasting sediment melt and fluid signatures for magmacomponents in the Aeolian Arc: Implications for numericalmodeling of subduction systems. Geochem. Geophys. Geosyst. 17 (6), 2034–2053.
Zhang, C., Liu, C.Z., Wu, F.Y., Zhang, L.L., Ji, W.Q., 2016a. Geochemistry and geochronology of mafic rocks from the Luobusa ophiolite, South Tibet. Lithos 245, 93–108.
Zhang, K.J., Xia, B.D., Wang, G.M., Li, Y.T., Ye, H.F., 2004. Early cretaceous stratigraphy. Depositional Environment, sandstone provenance, and tectonic setting of Central Tibet, western China. Geol. Soc. Am. Bull. 116 (9–10), 1202–1222.
Zhang, L.L., Liu, C.Z., Wu, F.Y., Zhang, C., Ji, W.Q., Wang, J.G., 2016b. Sr-Nd-Hf isotopes of the intrusive rocks in the cretaceous Xigaze ophiolite, southern Tibet: Constraints on its formation setting. Lithos 258–259, 133–148.
Zhang, S.Q., Mahoney, J.J., Mo, X.X., Ghazi, A.M., Milani, L., Crawford, A.J., Guo, T.Y.,Zhao, Z.D., 2005. Evidence for a widespread Tethyan upper mantle with Indian Ocean-Type isotopic characteristics. J. Petrol. 46(4), 829–858.
Zheng, H., Huang, Q., Kapsiotis, A., Xia, B., Yin, Z., Zhong, Y., Lu, Y., Shi, X., 2017. Early cretaceous ophiolites of the Yarlung Zangbo suture zone: Insights from dolerites and peridotites from the Baer upper mantle suite, SW Tibet (China). Int. Geol. Rev. 59 (11), 1471–1489.
Zhou, M.F., Robinson, P.T., Malpas, J., Edwards, S.J., Qi, L., 2005. REE and PGE geochemical constraints on the formation of dunites in the Luobusa Ophiolite, Southern Tibet. J. Petrol. 46 (3), 615–639.
Zhou, M.F., Robinson, P.T., Malpas, J., Li, Z., 1996. Podiform chromitites from the luobusa ophiolite (Southern Tibet): implications for melt/rock interaction and chromite segregation in the upper mantle. J. Petrol. 37, 3–21.